C.P. No. 869

C.P. No. 869

MINISTRY OF AVIATION

AERONAUTICAL RESEARCH COUNCIL

CURRENT PAPERS

Low-Speed Wind-Tunnel Measurements of Damping in Yaw ($n_{\dot{\psi}}$) on an A.R.9 Jet-Flap Complete Model

by

A. P. Cox and S. F. J. Butler

LONDON: HER MAJESTY'S STATIONERY OFFICE

1967

NINE SHILLINGS NET

U.D.C. No. 533.652.6 : 533.6.013.423 : 533.6.013.154 : 533.694.6

C.P. No. 869
February 1965

LOW-SPEED WIND-TUNNEL MEASUREMENTS OF DAMPING IN YAW ($n_{\dot{\psi}}$) ON AN ASPECT RATIO 9 JET-FLAP COMPLETE MODEL

by

A. P. Cox

S. F. J. Butler

SUMMARY

Measurements have been made of the yaw-damping derivative, $n_{\dot{\psi}}$, on an A.R.9 jet-flap complete model, using the free-oscillation technique. The experimental apparatus and procedure are fully described, with the exception of the special air-bearing support system, which has been the subject of a previous Report. Results are given of damping measurements at wing incidences of 0°, 10° and 20° with jet-flap control angles of 0° and 30° and a C_μ range of 0 to 4.2. The effects of the wing, fin, tailplane and fuselage were measured, and it was found that the latter gave a large and unpredicted destabilising contribution, while damping due to the fin was smaller than the estimated value. Visual observations of the flow in the jet wake showed some correlation with the measured effects.

Comparison of the measured damping for the complete wing + fuselage model with that estimated for the wing alone, assuming a full-span jet sheet, gave a deceptive measure of agreement, due mainly to the unexpectedly large fuselage contribution.

Replaces R.A.E. Technical Report No. 65021 - A.R.C. 27014

CONTENTS

		Page
1	INTRODUCTION	3
2	TEST ARRANGEMENT	4
	2.1 Model details	4
	2.2 Air-bearing assembly	5
3	EXPERIMENTAL METHOD	6
	3.1 Application of the free-oscillation technique	6
	3.2 Daily procedure	7
	3.3 Wing-alone tests	8
	3.4 Model behaviour and test accuracy	8
4	TEST RESULTS	9
	4.1 Preliminary tests	9
	4.2 Main series of tests	9
	4.2.1 Scope of main tests	9
	4.2.2 Basic wing + fuselage model	10
	4.2.3 The effect of a dorsal fin and fuselage spoiler	11
	4.2.4 The effect of the fuselage	11
	4.2.5 General discussion	12
5	COMPARISON OF RESULTS WITH ESTIMATES	13
	5.1 Method of estimation	13
	5.1.1 Estimation of $(n_r)_w$	14
	5.1.2 Estimation of $(n'_\psi)_f$	14
	5.2 Comparison between estimates and experimental results	15
6	CONCLUSIONS AND FURTHER WORK	16
Acknowledgments		16
Appendix A	Measurement of model oscillations	17
Appendix B	Calculation of n'_ψ from experimental results	19
Symbols		20
References		22
Illustrations		Figures 1-22
Detachable abstract cards		-

1 INTRODUCTION

In recent years, models of V/STOL aircraft employing various forms of jet blowing to attain high lift have formed the subject of extensive wind-tunnel tests, but this has included little work on the measurement of dynamic derivatives. The airflow characteristics can be entirely different from those associated with more conventional designs, with the possibility of large amplitudes of oscillation and important interference effects between the aircraft and associated engine jet efflux flows from the oscillating aircraft. A programme of model tests has started at R.A.E. to assess the validity of the application of quasi-steady treatments for derivative estimation on such configurations. An existing A.R.9 jet-flap complete model, which had already undergone extensive (conventional non-oscillatory) tests[1], was chosen for the initial experiments, largely because of the existence of elaborate theoretical treatments[2] for jet flaps. Also, the similarity between the model and the Hunting H126 research aircraft made the results useful, particularly for flight simulator studies, although the simplified fuselage shape was not representative of the aircraft and the aircraft fuselage jets were not simulated.

The choice of the yaw-damping derivative $n_{\dot{\psi}}$ (rotation about a fixed vertical axis) for measurement was influenced by various aerodynamic considerations. The main component of $n_{\dot{\psi}}$, namely n_r, was important because of the term $\ell_v n_r$ in the lateral stability determinant, particularly as unexpectedly large values of ℓ_v had already been encountered[1]. Moreover, the corresponding static derivative, n_v, had exhibited strong dependence on the sweepback of the wing and jet, so that the effect of the jet sheet on the fuselage and fin contribution could not be predicted, with any certainty, for an oscillating model. Where feasible, the present dynamic measurements have been compared with quasi-steady estimates.

The free-oscillation technique was adopted, not only because of its inherent simplicity for the measurement of a single direct damping derivative but also because the aerodynamic damping effects could more readily be appreciated over a representative range of amplitudes. In fact, a direct visual appreciation of the significance of the results was particularly valuable in the presence of the observed non-linear amplitude-dependent effects.

Naturally, the requirements of a jet blowing model complicated the experimental techniques for derivative measurement. The model was supported by an air-bearing assembly[3], enclosed within the fuselage which incorporated

the air connection for jet blowing, and was constrained by an arrangement of wires and springs. The method is basically suitable for use with other V/STOL wing-fuselage model arrangements.

The tests were made between February 1961 and April 1962, mainly in the R.A.E. No.2 $11\frac{1}{2}$ ft x $8\frac{1}{2}$ ft wind-tunnel, with a Reynolds number, $R\bar{c}$, of 0.32×10^6 at the principal test speed of 70 ft/sec.

2 TEST ARRANGEMENT

With use of the free-oscillation technique, the measured damping rates necessarily included contributions from the whole system, including the friction of the support bearings. If conventional mechanical bearings had been used, their friction could have contributed damping comparable with the expected aerodynamic damping. For this reason, and to facilitate the introduction of compressed air supplies for jet blowing, an air-bearing support system was adopted, having negligible friction. As discussed in Ref.3, a central bearing arrangement enclosed within the confines of the fuselage was chosen, rather than a much larger one built into the base of the strut carrying the model.

Principal details of the model and the air-bearing assembly are given in Sections 2.1 and 2.2 respectively. The method of recording the model motion is discussed fully in Appendix A, which also contains details of electrical devices used to provide automatic checks of the amplitude calibration and the internal damping.

2.1 Model details

The same wing, fin and tailplane were used as in the comprehensive steady tests of the aspect-ratio 9 jet-flap model. The wing was set at 4° dihedral with a wing-body angle of 5° and an unswept control hinge line. The new hollow fuselage, constructed from fibre-glass and epoxy resin, was half-an-inch bigger all round than the original solid wood fuselage of Ref.1.

The complete model is shown in Fig.1, together with a representative cross-section of the wing. The latter, of composite construction, employed a thick, highly cambered section (NACA 4424) to delay L.E. separations at high lift coefficients. The jet sheet emerged from the blowing slot in a direction parallel to the wing chord and impinged tangentially on the nose of the small, round-nosed, control surface. As in the previous tests, the slot width was tapered spanwise in proportion to the local wing chord to ensure a constant sectional momentum coefficient. Since internal airflow variations, occurring as the model oscillated, affected the spanwise distribution of jet

efflux, a tube with regulating holes along its length had to be inserted into each wing duct (see Fig.1). The area of the regulating holes was chosen to give choked conditions at the higher jet pressures. Because of the inclination of the upper surface of the control to the chord line, the effective jet-deflection angle (θ) was some 20° more than the nominal control setting (η). Control settings of 0° and 30°, corresponding to jet angles of about 20° and 50°, were used in the present tests.

The wings were joined together by a pair of plates sustaining the wing root bending moments and determining the wing dihedral setting (Fig.3). At its root, each wing carried a vertical side plate mounted on a spigot projecting from the outer body of the bearing. The spigots incorporated concentric airfeed connections to the wing, with 'O' ring seals to avoid air leaks. The wing incidence was preset by dowels joining mating holes in the sideplates and the bearing body. The central wing assembly also supported the fuselage shell and the tailplane spar.

For the measurement of wing damping in the absence of the fuselage*, the fuselage shells and tailspar were removed and the bearing assembly was enclosed by a stationary fairing (Fig.2). Slots were provided in the fairing to enable the wing to oscillate over an amplitude range of ±6°. A plasticine fillet was fixed to each wing at its root, affording a small clearance from the fairing, so that the slots in the latter were not uncovered as the wing oscillated.

2.2 Air-bearing assembly

The air-bearing assembly[3], shown installed in the model in Fig.3, consisted essentially of an inner component attached rigidly to the model support strut and an outer component moving with the model. Vertical forces due to the model weight and lift were supported by two annular air-bearing surfaces located in the drum-like lower part of the assembly. Drag and sideforce were supported by two cylindrical bearings, one forming the periphery of the drum and the other, of smaller diameter, located at the top of the assembly above the wing blowing duct entries. Pitching and rolling moments were sustained jointly by all four bearings. In order to support the maximum loads estimated from steady measurements, the bearing had to support a net vertical force (including model weight) of ±150 lb and, simultaneously, a combined drag and pitching moment load equivalent to a pitching moment of

*Extension of the jet sheet across the fuselage cut-out was not feasible with an internal air-bearing arrangement.

650 lb in. By careful adjustment of the bearing gaps, this load-carrying capacity was achieved[3] at the available supply pressure of 60 psig, with negligible internal damping.

The bearing assembly was capable of transmitting 2 lb/sec of air at 40 psig to the wings without any appreciable increase in its internal damping and without any throttling of the flow over an angular range of ±6°. A transducer was provided to measure the angle of rotation (ψ), in the form of a twin-ganged linear capacitor housed in the top of the bearing assembly.

3 EXPERIMENTAL METHOD

The use of the free-oscillation technique is usually straight-forward and reliable, provided that the friction of the bearing support is low (see para.2.2 and Appendix A) and the restraining spring arrangement is satisfactory (see para.3.1). Considerable care was taken, with calibration checks included in the normal running procedure (see para.3.2), and a special arrangement was devised for some additional tests with the wing alone (see para.3.3). However, not only were the observed aerodynamic damping effects strongly dependent on amplitude, but also there was some lack of repeatability, with consequent effects on the feasible test accuracy (see para.3.4).

3.1 Application of the free-oscillation technique

The model support strut was bolted to a rigid structure below the tunnel floor. Springs were attached to vertical beams bolted to the tunnel structure on either side of the working section and connected by 24 SWG steel wires to flexure hinges on the tail spar some 20 inches behind the pivot of the model. The flexure hinges were fabricated from 0.006 inch shim soldered into end fittings. These flexures, which were more flexible than those produced by the normal method of machining from the solid, were quick and easy to manufacture, yet proved quite satisfactory in service. To prevent aerodynamically excited wire oscillations, the wires were screened from the mainstream air flow over most of their length by 1 inch diameter tubes (Fig.6). A range of springs enabled periods of oscillation of approximately 1, 2 and 5 seconds to be obtained.

The moment of inertia, C, of the model was determined by measuring its period of oscillation, with and without an additional mass on each wing tip, the weights having a known increment of inertia, C_1. Thus, if T_1 is the period of oscillation for model + weights and T is the corresponding value without weights, then

$$C = C_1 T^2/(T_1^2 - T^2) \quad .$$

For tests without fin, a lead weight was added to maintain the same total moment of inertia. Because of space limitations, it was not readily possible to compensate for the absence of the tailplane in the same way and so both the moment of inertia and period of oscillation were slightly greater for the tests with a tailplane.

3.2 Daily procedure

Although the model was fitted with an automatic check of the yaw angle calibration (see Appendix A), a daily check of its accuracy was made. For this purpose, a pointer was attached to a wing tip moving over a scale fixed on a stand located by holes drilled in the tunnel floor. After an initial warming-up period, a trace of a few oscillations was taken to record the $\pm 3^{\circ}$ triggering points and the model was then held at scale positions of 0°, $+3^{\circ}$ and -3° in turn.

The wind-off damping due to the model and rig was determined from measurements of the time taken for model oscillations to damp from an amplitude of $\pm 6^{\circ}$ to $\pm 2.2^{\circ}$ ($\bar{V}_0$ to $\bar{V}_0/e$).

The normal running procedure was as follows:-

(a) The blowing pressure corresponding to the desired value of C_μ was set.

(b) The wind-tunnel speed was set at the prescribed value, and the spring attachment bolts were adjusted to remove any yaw on the model* due to asymmetric thrust or aerodynamic moment.

(c) With positive damping, the model was manually forced by pulling cyclically on one of the wire/spring junctions until the amplitude was greater than $\pm 6^{\circ}$, when the model was carefully released and the recorder started**. The run was continued until the oscillations had damped out completely or had reached a small, steady, residual amplitude (usually not more than $\pm 1^{\circ}$).

(d) For conditions of near-zero damping, representative traces were obtained at several amplitudes.

---

*The effect of small asymmetries of thrust were quite considerable for the model without fin with the weak springs fitted ($T = 5$ sec), and provided a lower limit to the strength of springs that could be used. In fact, it would have been preferable to increase the moment of inertia, rather than reduce the spring strength, in order to attain very low frequencies of oscillation.

**The alternative method of pulling the model 6° to one side and releasing it was found to cause unacceptable spring vibrations, which prevented accurate trace measurements until an appreciably lower amplitude had been attained.

(e) In the presence of negative damping, the model was released from rest at zero yaw and the ensuing motion observed within the available amplitude range.

Each run was repeated at least once, depending on the type of motion. Often, several repetitions were necessary because of aerodynamic difficulties associated with the model behaviour (see Section 3.4).

3.3 Wing-alone tests

The measurement technique employed for wing-alone tests was identical, except that the springs were attached much closer to the pivot axis and in front of the wing. Thus, much greater spring strengths were required for the same period of oscillation as before, and the minimum practicable period was 4 seconds.

As described in para.2.1, the structure at the centre of the model was enclosed within a stationary container, with slots cut in it to allow for the passage of the wires to the springs and to enable the wing to oscillate. As these slots had to be as small as possible, they were made just big enough to allow an amplitude of $\pm 6^{\circ}$ although accurate trace measurements was limited to a rather smaller amplitude. Due to lack of space, the automatic amplitude calibration equipment was removed, but the "bearing freedom" circuit was retained (see Appendix A).

3.4 Model behaviour and test accuracy

A cautious approach to the analysis and presentation of the results was adopted, because of the amount of scatter and the general nature of the test behaviour. Comparison of the results for different model configurations (e.g. fin-on versus fin-off) showed that the basic accuracy was reasonable, particularly when the aerodynamic damping was pronounced. However, in addition to some lack of repeatability from one run to another, variations in damping were often encountered in a particular run (see Fig.7). Furthermore, the damping rate clearly depended on amplitude. This feature was particularly evident if the aerodynamic damping was low, when positive damping at large amplitudes was accompanied by reduced, or even negative damping at the lower amplitudes. A long-period disturbance was sometimes observed which, under such conditions, led to a regular build-up and decay of amplitude. Precise determination of the damping rate at a particular amplitude was then difficult and variations between individual results were inevitable.

The frequency of the long-period disturbance suggested the possibility of self-excitation due to small amplitude flow disturbances persisting around

the tunnel return circuit. However, no evidence of this was found from measurements of yaw fluctuations ahead of the model. It was therefore concluded that the non-linear effects were associated directly with the flow around the model, rather than the time history of the tunnel mainstream.

The values of $n_{\dot{\psi}}$ were derived from trace records for a restricted amplitude range of 6° to 4°, where the effects of the non-linearities were less noticeable. In addition to the individual results, the overall distribution of results has been indicated using shaded areas, as well as mean curves. Despite reservations as to the accuracy of individual results, the trends of the mean curves are well substantiated. Regarding extrapolation to full-scale conditions, Reynolds number effects seem likely, particularly in view of the importance of the fuselage contribution.

4 TEST RESULTS

4.1 Preliminary tests

The first series of tests, in the R.A.E. No.1 $11\frac{1}{2}$ ft x $8\frac{1}{2}$ ft wind-tunnel was exploratory in nature. Some very high values of damping were measured, which were later attributed to overloading of the air-bearing; as a consequence, the electrical indication of bearing friction mentioned in Appendix A was incorporated. Little effect was found on changing the quality of the tunnel airstream, by removing the tunnel honeycomb which was present for most of these initial tests (Fig.8a). However, it was decided that the No.2 $11\frac{1}{2}$ ft x $8\frac{1}{2}$ ft wind-tunnel, which has a lower turbulence level and longer return circuit, should be used for the remaining tests. The second test series was curtailed by equipment faults, with little time for actual measurements. However, the effect of the main parameters was explored and it was confirmed that the more extreme damping rates measured in the first tests were erroneous. The results of these preliminary tests, in general, were confirmed (see Fig.8) by the main series of tests discussed in the next section.

4.2 Main series of tests

4.2.1 Scope of main tests

A range of blowing pressures was used in the main tests, which covered C_{μ}-ranges of 0 to 4.2, 0 to 2.1 and 0 to 0.43 at tunnel speeds of 50, 70 and 140 ft/sec respectively. Particularly at the highest speed, the C_{μ}-range was limited at times by deterioration in the load capacity of the air-bearing. For most of the tests, a period of oscillation, T, of 2 seconds was employed, with variation between 1 and 5 seconds in specific cases. As explained in para.3.2

and para.3.4, the values of $n_{\dot{\psi}}$ have been derived for an amplitude range of 6° to 4°.

With the basic wing-fuselage model*, tests were made at α_w = 0°, 10° and 20° for control angles of 0° and 30°, both with and without the fin; the effect of adding the tailplane to the fin was also determined (see Section 4.2.2.). Some additional tests, at α_w = 0°, with a dorsal fin and with a fuselage spoiler are described in Section 4.2.3.

Tests of the wing alone (see Section 4.2.4), with the usual control angles of 0° and 30°, were limited to α_w = 0°. As the maximum practicable time period was 4 seconds (see Section 3.3), the required C_μ range was obtained with the prescribed frequency parameter range by using an additional test speed of 30 ft/sec.

Some visual studies of the flow field through which the fuselage and fin moved were also attempted, together with some measurements of the static pressure variations on the side of the fuselage and the fin (see Section 4.2.5).

4.2.2 Basic wing + fuselage model

The influence of the frequency parameter, $\omega(= \pi b/TV_o)$, on the variation of $n_{\dot{\psi}}$ with C_μ for V_o = 70 ft/sec, is shown in Fig.9. In view of the comparative insensitivity to this parameter**, the systematic tests (see Figs.10-12) were made at T_{nom} = 2 seconds, with variation of C_μ by jet pressure ratio and V_o. The wing Reynolds number, although low, had no apparent effect over the range tested (0.23×10^6 to 0.64×10^6).

For η = 0° ($\theta \simeq 20°$), $n_{\dot{\psi}}$ did not vary appreciably with C_μ but tended to become more negative (increased damping) on increase of wing incidence (Figs.10a, 11a and 12a). The fin contribution to $n_{\dot{\psi}}$ at η = 0° decreased gradually with increase in C_μ but was not sensitive to α_w (see Section 5.2 and Figs.13, and 21a).

For η = 30° ($\theta \simeq 50°$), however, the variations of $n_{\dot{\psi}}$ with C_μ were more complicated (Figs.10b, 11b and 12b). As C_μ was increased from zero to the value for attachment of about 0.1, there was a sharp decrease in the damping rate as

---

*Unless otherwise stated, it should be assumed that the text and figures refer to this configuration.

**For jet-blowing models, it is arguable that the frequency parameter should be based on V_J rather than V_o; in the present case, it is clear that the alternative parameter is also of no great significance.

the flow over the flaps became fully attached. With further increase in C_μ, there was a gradual increase in damping except at $C_\mu \simeq 2$, where there was a further sudden decrease, particularly when $\alpha_w = 10^\circ$. The fin contribution for $\eta = 30^\circ$ was generally much smaller than at $\eta = 0^\circ$, and became negligible at $\alpha_w = 20^\circ$ (see Figs.13 and 21b).

Some increase in the magnitude of the fin contribution would be expected on addition of the tailplane, as a result of increased fin effectiveness. However, some tests of the effect of the tailplane* did not show a consistent effect on the fin contribution to $n_{\dot{\psi}}$ except, possibly, at $C_\mu = 0$ (see Fig.13).

4.2.3 The effect of a dorsal fin and a fuselage spoiler

Often the trace records showed a well-defined superimposed long-period disturbance (see Section 3.4). A similar tendency for cyclic variations of damping rate was found in previous oscillatory tests on a model of the Meteor III[4], corresponding to "snaking" of the aircraft. In that case, it was found that a "rope" spoiler around the nose of the model effectively eliminated such behaviour. A similar device fitted to the present model had no significant effect on the linearity of damping although increasing the damping rate slightly at low values of C_μ (Fig.14).

A dorsal fin, as fitted to the Hunting H126 aircraft, was found to cause a slight reduction in damping (Fig.14), which can be compared with the destabilising effect of the fuselage itself (see next section).

4.2.4 The effect of the fuselage

As a result of the tests of the basic wing + fuselage model, it was decided to attempt tests of the wing alone. It was, of course, appreciated that the test arrangement was far from ideal, not only because of the necessity for a stationary fairing, but also because of the part-span nature of the jet efflux. With the wing alone, there was considerable scatter at the higher C_μ-values (see Fig.15), apparently due to the overall changes in damping rate rather than non-linearity, as encountered with the basic wing + fuselage model. Although there was possibly some evidence that a decrease in the damping rate still accompanied flow attachment over the controls at $\eta = 30^\circ$, there was no sign of the second decrease at $C_\mu \simeq 2$ observed at this control angle in the presence of the fuselage.

Comparison between the results of the basic tests and the wing-alone tests (Fig.16) shows not only that the fuselage contribution was destabilising,

*At tailplane settings chosen to give $C_{L_{tail}} \simeq 0$.

but also that it was comparable with the stabilising fin contribution (Figs.21 and 22).

4.2.5 General discussion

Conventional estimates of the fuselage damping contribution, based on fuselage side area considerations, predict a small, stabilising contribution in contrast to that measured in the present experiments. Further, the present results for $C_\mu \simeq 2$ with $\eta = 30^\circ$, $\alpha_w = 0^\circ$ and 10°, strongly suggested abrupt flow changes in the airflow around the basic model. The previous static stability tests had shown rather similar effects on n_v, when the wing sweepback was increased by 10° so that the jet sheet and trailing-vortex system were in close proximity to the sides of the fuselage. In order to obtain further understanding of the nature of the interaction for the oscillating model, the behaviour of the trailing vortices originating in the wing root junction was studied by trailing streamers, carrying small plastic discs at frequent intervals, and surface tufts were attached to the rear fuselage.

At $\eta = 30^\circ$, $\alpha_w = 0^\circ$, the inboard vortices stayed along wind at low values of C_μ, but oscillated with the model at C_μ-values above 1.0, with a fairly abrupt transition. At $\eta = 30^\circ$, $\alpha_w = 10^\circ$, the flow change occurred at $C_\mu \simeq 1.7$ but was less clearly defined. On the other hand, with $\eta = 0^\circ$, the vortices oscillated with the model throughout the C_μ-range.

The fuselage tufts showed areas of flow separation* and downwash changes on the rear fuselage which varied in extent as the model oscillated. Generally, the area of separation on the "leeward" side was greater. At $C_\mu = 0$, marked downwash changes occurred on the fuselage sides during oscillation, associated with the relative movements of the wing-root vortices.

The strength of the wing-root vortices, as well as the tip vortices, is much increased at the high C_L-values associated with a jet flap wing. Moreover, calculations by Thomas[2] show that the distance behind the wing, d, at which the rolling-up of the jet sheet is essentially complete, is given by

---

*To ascertain whether such separations were primarily due to the wing and jet, or to strut interference, the fuselage was mounted separately on wire, with a simulated dummy strut. The effects of the strut were shown to be limited to the area of the fuselage immediately behind it, thus confirming that the major separated areas on the fuselage were due to wing and jet wake effects.

$$\frac{d}{b} = \frac{K^*}{2C_L} \quad \text{(where } K^* \text{ is a constant depending on the planform)}$$

$$= \frac{0.28A}{C_L} \quad \text{for elliptic loading}$$

Thus, as the lift coefficient is increased, the rolling-up process is completed more rapidly and strong vortices in the neighbourhood of the rear fuselage must be expected. The damping contribution from the fuselage and fin might reasonably be expected to depend greatly on the relative strength, orientation and stability of these vortices.

To assist further understanding, the variation in static pressure differential between points on either side of the rear fuselage was measured by a capacitive pressure transducer, connected to the trace recorder to allow direct correlation with the angle of yaw. Although surface pressure variations were confirmed, it was not found possible to obtain regular curves with cyclic variations suitable for quantitative analysis. Similar measurements at the maximum thickness position of the fin were more successful and showed sinusoidal variations, with a phase relationship of the correct sign. However the magnitude of the phase difference was rather large in comparison with the measured fin-damping contribution. Some form of integration of the out-of-phase static pressure component would seem necessary to achieve a reasonably accurate correlation.

5 COMPARISON OF RESULTS WITH ESTIMATES

5.1 Method of estimation

The derivative, $n_{\dot{\psi}}$, measured by oscillating a model about a fixed, vertical wind axis, is made up of two components,

$$n_{\dot{\psi}} = n_r - n_{\dot{v}} \qquad (1)$$

where n_r is the yawing moment due to rate of yaw ($n_r = \partial C_n/\partial(rb/2V_o)$) and $n_{\dot{v}}$ is the yawing moment due to acceleration in sideslip ($n_{\dot{v}} = \partial C_n/\partial(\dot{v}b/2V_o)$), n_r is composed of contributions from the wing, fuselage and fin, while $n_{\dot{v}}$ is largely due to the fin only. In practice, the fuselage contribution to n_r is generally ignored as being negligible, even though an empirical analysis by, Pinsker[5] has shown that the fuselage contribution is often comparable to that of the fin. Unfortunately, this method predicts a negative contribution to n_r, and did not seem applicable to this particular aerodynamic configuration.

Hence, the estimated value of $n_{\dot{v}}$ was derived ignoring the fuselage contribution to n_r, i.e.,

$$n_{\dot{v}} = (n_r)_w + ((n_r)_f - (n_{\dot{v}})_f) = (n_r)_w + (n_{\dot{v}})_f \quad . \tag{2}$$

5.1.1 Estimation of $(n_r)_w$

The contribution $(n_r)_w$ has been calculated using the method of Thomas and Ross[2] for a jet flap wing. This assumes a full-span jet sheet, uninterrupted by a fuselage, and is based on quasi-steady flow conditions with straight, and not curved, trailing vortices. Then $(n_r)_w$ is given by the relation

$$(n_r)_w = (n_r)_i + (n_r)_o \quad , \tag{3}$$

where the induced drag contribution,

$$(n_r)_i = -\frac{3\bar{C}_L^2}{8\pi A}\left\{\frac{\pi A}{\pi A + 2C_\mu}\right\}^2 \frac{(1 + 32C_\mu/9\pi A)}{(\pi A + 2\mu_2 + 2C_\mu \mu_1)} \times$$

$$\times \left\{\pi A + \mu_2 + C_\mu \dot{\mu}_1 + 2(C_\mu \dot{\mu}_2 + C_\mu^2 \ddot{\mu}) - \frac{2C_\mu}{C_{L\infty}} (\pi A + \mu_2 + C_\mu \dot{\mu}_1) \frac{\partial C_{L\infty}}{\partial C_\mu}\right\} \quad , \tag{4}$$

and the profile drag contribution,

$$(n_r)_o = -C_{Dc}/4 \quad . \tag{5}$$

5.1.2 Estimation of $(n_{\dot{v}})_f$

The effective flow direction at the fin in sideslip may be regarded as the sum of the components due to the sidewash, the rate of change of sidewash with time, and steady rate of yaw.

Then

$$\beta_{eff} = \beta + (\partial\sigma/\partial\beta)\beta - (\partial\sigma/\partial\beta)\,(\partial\beta/\partial t)\tau - r\,\ell_f/V_o \tag{6}$$

where τ is the time lag arising from the distance between the wing and fin, and so may be approximated by $\tau = \ell_f/V_o$.

The yawing moment due to the fin is

$$N_f = \tfrac{1}{2}\rho V_o^2 S_f \ell_f (a_1)_f \beta_{eff}$$

and the yawing moment coefficient, $(C_n)_f$, is

$$(C_n)_f = N_f/\tfrac{1}{2}\rho V_o^2 Sb$$

$$= (S_f/S)\ (\ell_f/b)\ (a_1)_f\ \beta_{eff} \quad . \tag{7}$$

The associated derivatives may be obtained by partial differentiation

$$(n_v)_f = \partial(C_n)_f/\partial\beta = (S_f/S)\ (\ell_f/b)\ (a_1)_f\ (1 + \partial\sigma/\partial\beta) \tag{8}$$

$$(n_r)_f = \partial(C_n)_f/\partial(rb/2V_o) = -2(S_f/S)\ (\ell_f/b)^2\ (a_1)_f \tag{9}$$

$$(n_{\dot v})_f = \partial(C_n)_f/\partial(\dot v b/2V_o) = \partial(C_n)_f/\partial(\dot\beta b/2)$$

$$= -2(S_f/S)\ (\ell_f/b)^2\ (a_1)_f\ (\partial\sigma/\partial\beta) \tag{10}$$

and

$$(n_{\dot\psi})_f = (n_r - n_{\dot v})_f \tag{11}$$

On eliminating $(\partial\sigma/\partial\beta)$ in terms of $(n_v)_f$, which may be obtained from wind-tunnel measurements, the expression for $(n_{\dot\psi})_f$ reduces to

$$(n_{\dot\psi})_f = -4(S_f/S)\ (\ell_f/b)^2\ (a_1)_f + 2(n_v)_f\ (\ell_f/b) \quad . \tag{12}$$

5.2 Comparison between estimates and experimental results

The estimated value of $n_{\dot\psi}$ for the complete model, both with and without the fin, is compared with the distribution of measured values for the basic wing + fuselage model in Figs.17-19. The results without the fin are summarised in Fig.20, including measurements on the isolated wing. In these comparisons, it must be remembered that the theory does not make any allowance for the discontinuous jet sheet or the fuselage. Nevertheless, there is some measure of broad agreement, with the exception of the case $\eta = 30^o$, $\alpha_w = 10^o$, $C_\mu > 2$. However, in view of the apparent size of the fuselage contribution (see Section 4.2.4), such agreement between the estimates and the basic (wing + fuselage) model would appear to be quite fortuitous. As an alternative, a comparison may be made with the wing-alone results (Fig.20). In this case, the agreement is tolerable only at high C_L-values and $\eta = 30^o$. But the theory is not necessarily invalidated, in view of the presence of a central fairing and the discontinuous nature of the jet sheet.

To allow a reliable comparison with the present theory, there appears to be no alternative to further tests on the wing-alone modified to provide a full-span jet sheet. Obviously, an extension to the theory, to allow for the effect of a part-span jet sheet and a fuselage, is desirable to facilitate estimates for practical aircraft configurations.

The need for further theoretical treatments is confirmed by the comparison between measured and estimated fin contributions (see Fig.21). Although fair agreement was obtained at $\eta = 0^{\circ}$, the measured contributions at $\eta = 30^{\circ}$ were much smaller than the estimates.

In view of the size of the fuselage contribution and the nature of the jet sheet-fuselage interactions, some care is advisable when considering applications of the present results to the Hunting H126 jet flap research aircraft, which has fuselage side jets as well as a rather different fuselage shape. There is, of course, the additional possibility of significant Reynolds number effects. In view of the probable sensitivity to aircraft layout, the likely accuracy of present theoretical treatments for the fuselage and fin contributions seems to be rather limited, and some recourse to experiment is needed at this stage.

6 CONCLUSIONS

Measurements of the damping derivative in yaw, $n_{\dot{\psi}}$, have been made on a jet-flap wing-fuselage model by the free-oscillation technique, using an internal air-bearing support arrangement. Damping characteristics were measured at wing incidences of 0°, 10° and 20° with jet-flap control angles of 0° and 30° and a C_{μ}-range of 0 to 4.2. The effects of the wing, fin tail-plane and fuselage were obtained, and it was found that the latter gave a large and unpredicted destabilising contribution, while damping due to the fin was smaller than the estimated value. The aerodynamic damping effects were strongly dependent on amplitude, with some lack of repeatability.

Acknowledgments

The authors are grateful to Hunting Aircraft Limited, for providing assistance with the analysis of the test results.

Appendix A

MEASUREMENT OF MODEL OSCILLATIONS

The signal from an F.M. oscillator, modulated by the capacitance variations of the yaw transducer, was amplified and then fed into a discriminator. The voltage output was directly proportional to the change in capacitance of the transducer from its mean position, and hence varied linearly with the angular displacement of the model. The output was applied to one channel of an ultra-violet trace recorder (Fig.4).

Although the equipment generally maintained its calibration, on one occasion in early tests the calibration suddenly changed and then reverted to its original value. Subsequently, a second channel on the trace recorder was used to provide a combined check of changes in instrument calibration and internal friction. Fig.4 shows the arrangement of circuit components and Fig.3 illustrates the installation of the calibration equipment in the model. Bearing overload was detected by measuring the electrical resistance between the moving and static components of the bearing. This resistance, which was virtually infinite when the bearing was floating freely, fell to a very low value whenever metallic contact occurred. The bearing resistance was recorded by the second channel in the trace recorder through a resistance (R_1) from a 1.5V battery, which deflected the trace from its "zero" position at A (Fig.5) to B. The bearing was connected across the recorder input so that contact between the bearing surfaces short-circuited the recorder galvanometer, causing the trace to return to A. A continuous record was thus provided of the state of freedom of the bearing.

Automatic calibration checks were effected by recording the instant at which the model passed through points nominally at $\pm 3^\circ$ yaw. Fig.3 shows the two sensing units, each of which consisted of a metal block containing a 12V bulb and a photo-transistor connected by a 1/16 inch diameter hole. The units were spaced at $\pm 3^\circ$ to the horizontal axis on a plate fixed to the stationary part of the bearing, with a shutter, which had a narrow vertical aperture at its centre, attached to the moving component (see Figs.3 and 4). As the model oscillated through a half cycle, the appropriate photo-transistor provided two current pulses as the aperture passed first one way, and then the other, through the 3° point. To eliminate the second pulse of each pair, the outputs from the two photo-transistors were amplified and connected to the inputs of a bistable circuit controlling a relay, R_L. From each positive excursion of ψ through $+3^\circ$ to each negative excursion through -3°, the relay switched a high

resistance into the electrical circuit between the bearing faces, causing a step in the "bearing-freedom" trace (e.g., B to C, Fig.5). Thus the time instants at which the trace steps occurred corresponded to the passage of the model through $\pm 3^{\circ}$ yaw.

Appendix B

CALCULATION OF $n_{\dot{\psi}}^{\bullet}$ FROM EXPERIMENTAL RESULTS

With a freely-pivoted model constrained by springs and executing an exponentially-damped harmonic motion, then

$$\psi(t) = \psi_c e^{N_{\dot{\psi}}^{\bullet} t/2C} \cos(2\pi t/T) \quad .$$

With the peak amplitude envelope defined by

$$\bar{\psi}(t) = \bar{\psi}_c e^{N_{\dot{\psi}}^{\bullet} t/2C}$$

so that

$$N_{\dot{\psi}}^{\bullet} = 2C\, \partial(\log \bar{\psi}(t))/\partial t \quad .$$

In non-dimensional form,

$$n_{\dot{\psi}}^{\bullet} = N_{\dot{\psi}}^{\bullet}/(1/4\rho V_c S b^2) \quad .$$

SYMBOLS

$(a_1)_f$ fin lift-curve slope

A wing aspect ratio

b wing span

C moment of inertia of model about yaw axis

C_1 known increment of inertia added to model

C_{Do} wing profile drag coefficient = $D_o/q_c S$

C_ℓ rolling moment coefficient = ℓ/q_o Sb

C_L lift coefficient = L/q_o S

$\bar{C}_L$ total lift coefficient

$C_{L\infty}$ lift coefficient of infinite span wing

C_n yawing moment coefficient = N/q_c bS

C_μ jet momentum coefficient = $M_J V_J/q_c$ S

d distance behind wing at which rolling-up of vortex sheet is complete

ℓ_f fin arm

ℓ_v rate of change of rolling moment coefficient with sideslip = $\partial C_\ell/\partial\beta$

M_J measured mass-flow rate

n_r yawing moment derivative due to yawing = $\partial C_n/\partial \left(\frac{rb}{2V}\right)_o$

$(n_r)_f$ increment of n_r due to fin (no tailplane)

$(n_r)_i$ the part of n_r due to induced drag

$(n_r)_o$ the part of n_r due to profile drag

$(n_r)_w$ increment of n_r due to the wing

n_v rate of change of yawing moment with sideslip = $\partial C_n/\partial\beta$

$n_{\dot{v}}$ rate of change of yawing moment with rate of sideslip = $\partial C_n/\partial \dot{\beta}$

$(n_{\dot{v}})_f$ increment of $n_{\dot{v}}$ due to fin (no tailplane)

n_ψ yawing moment derivative due to yawing about a fixed wind axis = $(n_r - n_{\dot{v}})$

$(n_\psi)_f$ increment of n_ψ due to fin

N_r dimensional yawing moment derivative due to yawing = $\partial N/\partial r$

$(N_r)_f$ increment of N_r due to fin

N_ψ dimensional yawing moment derivative about a fixed axis

q_o mainstream dynamic head

SYMBOLS (CONTD.)

r	rate of yaw
S	gross wing area
S_f	fin area
t	time for amplitude of oscillations to decay from $\bar{\psi}_o$ to $\bar{\psi}$
T	period of oscillation of model
T_1	period of oscillation of model with additional moment of inertia, C_1
v	sideslip velocity
V_o	mainstream speed
V_J	jet speed
α_w	wing incidence
β	angle of sideslip
η	angle of deflection of jet flap control
θ	effective jet deflection angle
μ_1	$\partial C_{L\infty}/\partial\theta$, a function of C_μ only
μ_2	$\partial C_{L\infty}/\partial\alpha$, a function of C_μ only
σ	angle of sidewash at fin
τ	time lag of mainstream flow between wing and fin
ψ	angle of yaw
$\bar{\psi}_o$	initial amplitude of oscillations ($t = 0$)
$\psi(t)$	angle of yaw after time, t
$\bar{\psi}(t)$	amplitude of oscillation after time, t
ω	reduced frequency parameter $= \pi b/TV_o$

REFERENCES

No.	Author	Title, etc.,
1	S. F. J. Butler H. B. Guyett B. A. Moy	Six-component low-speed tunnel tests of jet flap complete models with variation of aspect ratio, dihedral, and sweepback, including the influence of ground proximity. (A.R.C. R&M 3441), June 1961
2	H. H. B. M. Thomas A. J. Ross	The calculation of the rotary lateral stability derivatives of a jet-flapped wing. (A.R.C. R&M No.3277), January 1958
3	A. P. Cox	The design and development of an air-bearing for the measurement of damping in yaw on a jet-blowing model. (A.R.C. C.P. No. 796), April 1964
4	J. G. Ross R. C. Lock	Wind-tunnel measurements of yawing moment due to yawing (n_r) on a 1/5.5 scale model of the Meteor Mark FIII. (A.R.C. R&M No. 2791), May 1947
5	W. J. G. Pinsker	Fuselage contribution to the damping in yaw. Unpublished M.O.A. work, 1951

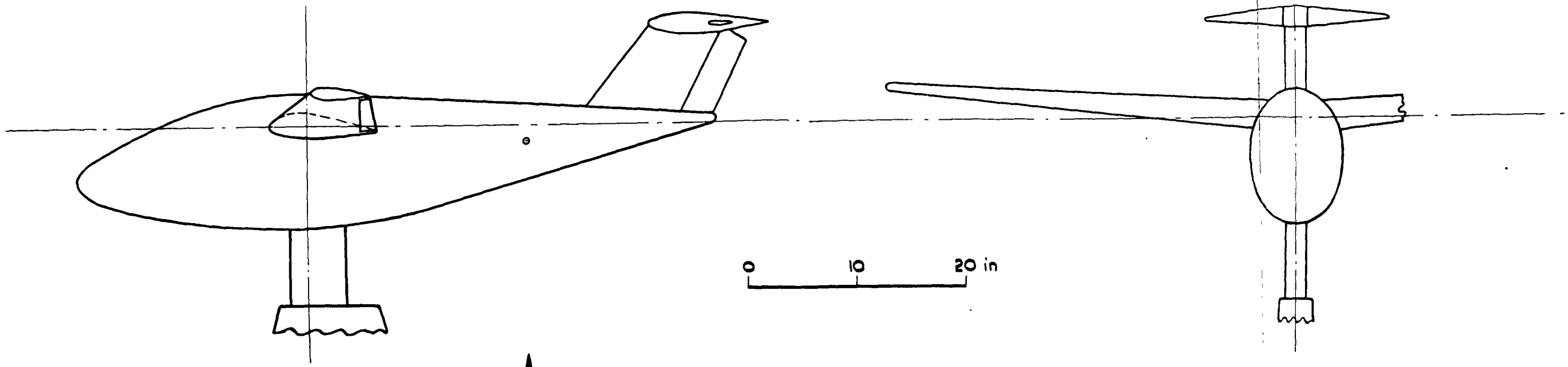

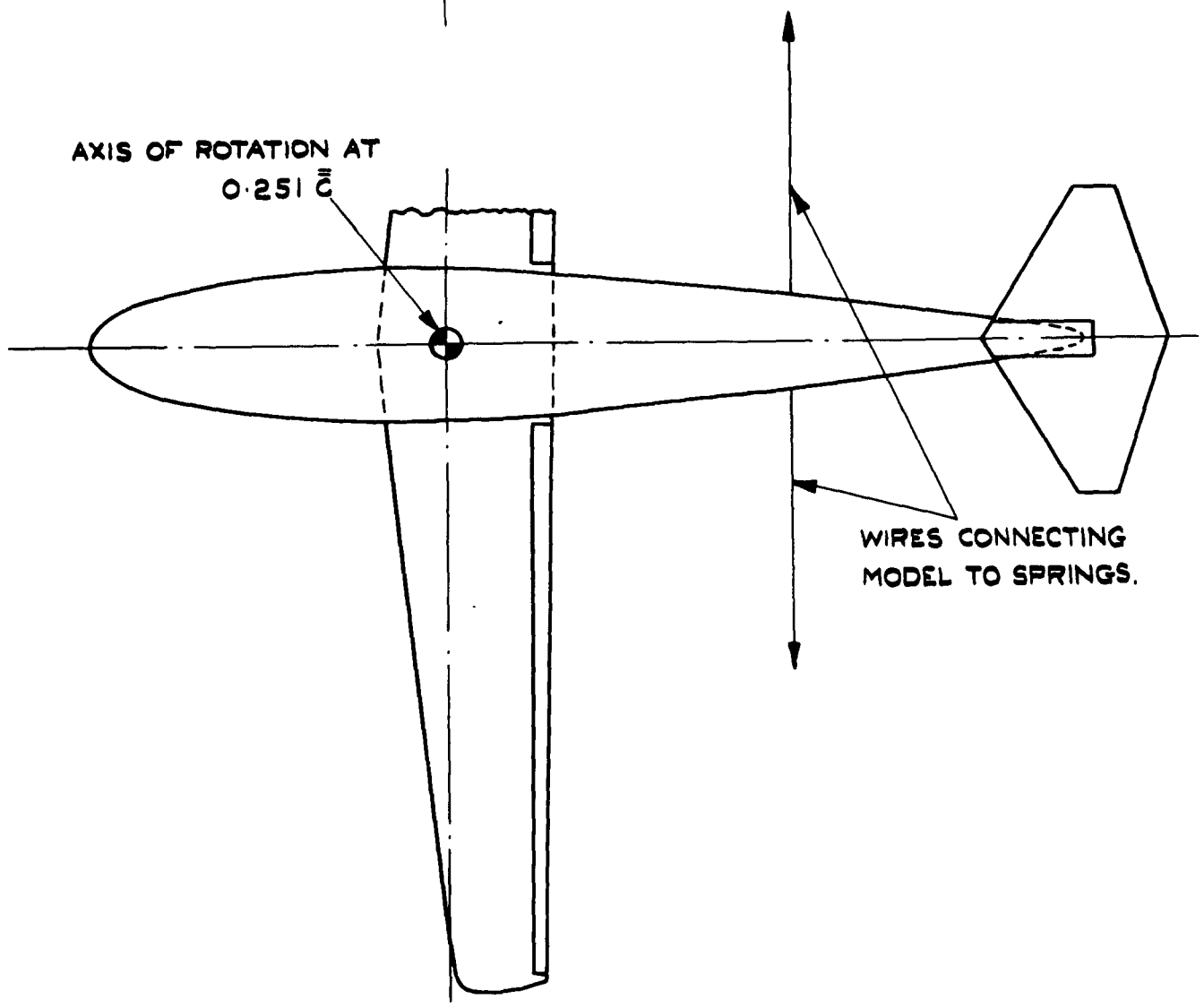

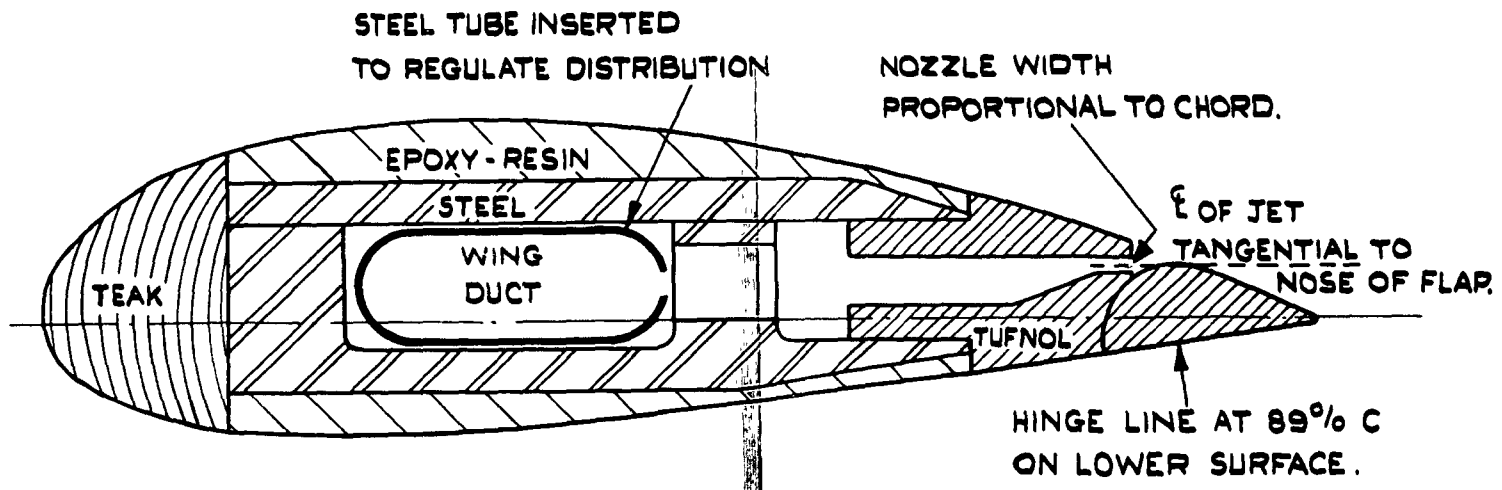

WING SECTION AT 26·33 in FROM CENTRE-LINE (NACA 4424)
(FULL MODEL SCALE)

DETAILS OF MODEL

S	604·5	sq in
b	74·50	in
C_{ROOT}	11·00	in
C_{TIP}	5·33	in
$\bar{C}$	8·09	in
$\bar{\bar{C}}$	8·46	in
A.R.	9·20	in

T.R.	0·485
WING/BODY ANGLE	5°
QUARTER-CHORD SWEEP	6°
HINGE-LINE SWEEP	0°
DIHEDRAL	+4°
S_t	122·3 sq in
l_t	36·0 in

FIG. 1. GENERAL ARRANGEMENT OF A.R.9. JET-FLAP MODEL.

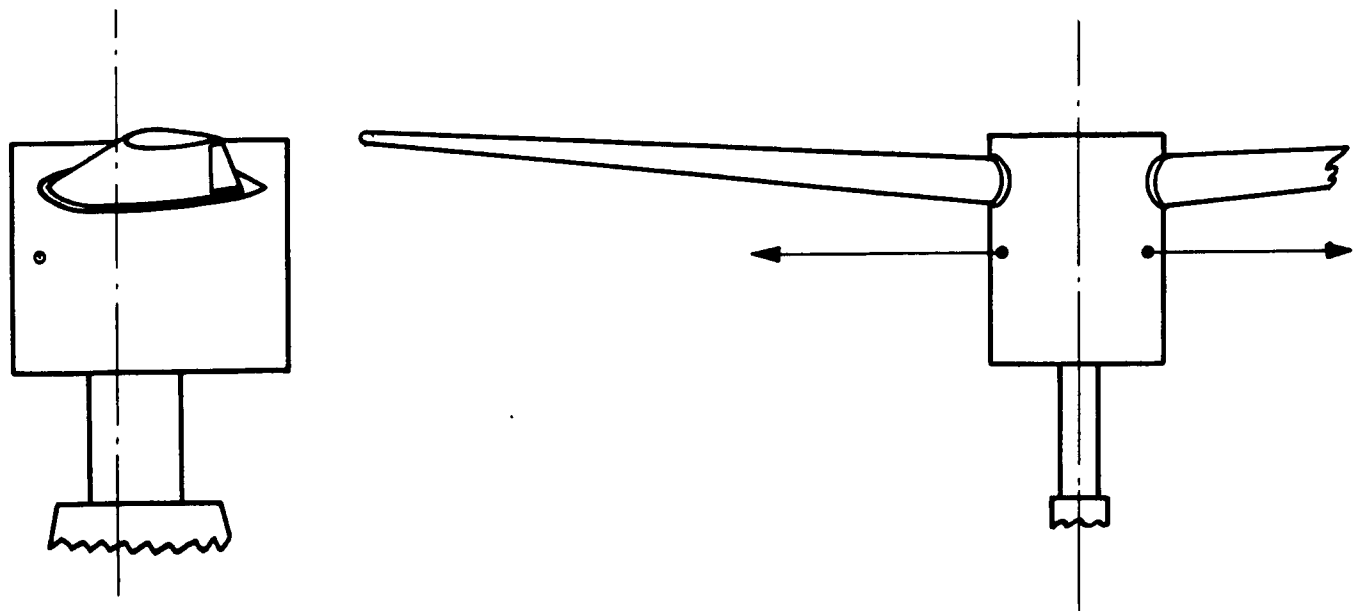

FIG. 2. MODEL ARRANGEMENT FOR WING-ALONE TESTS.

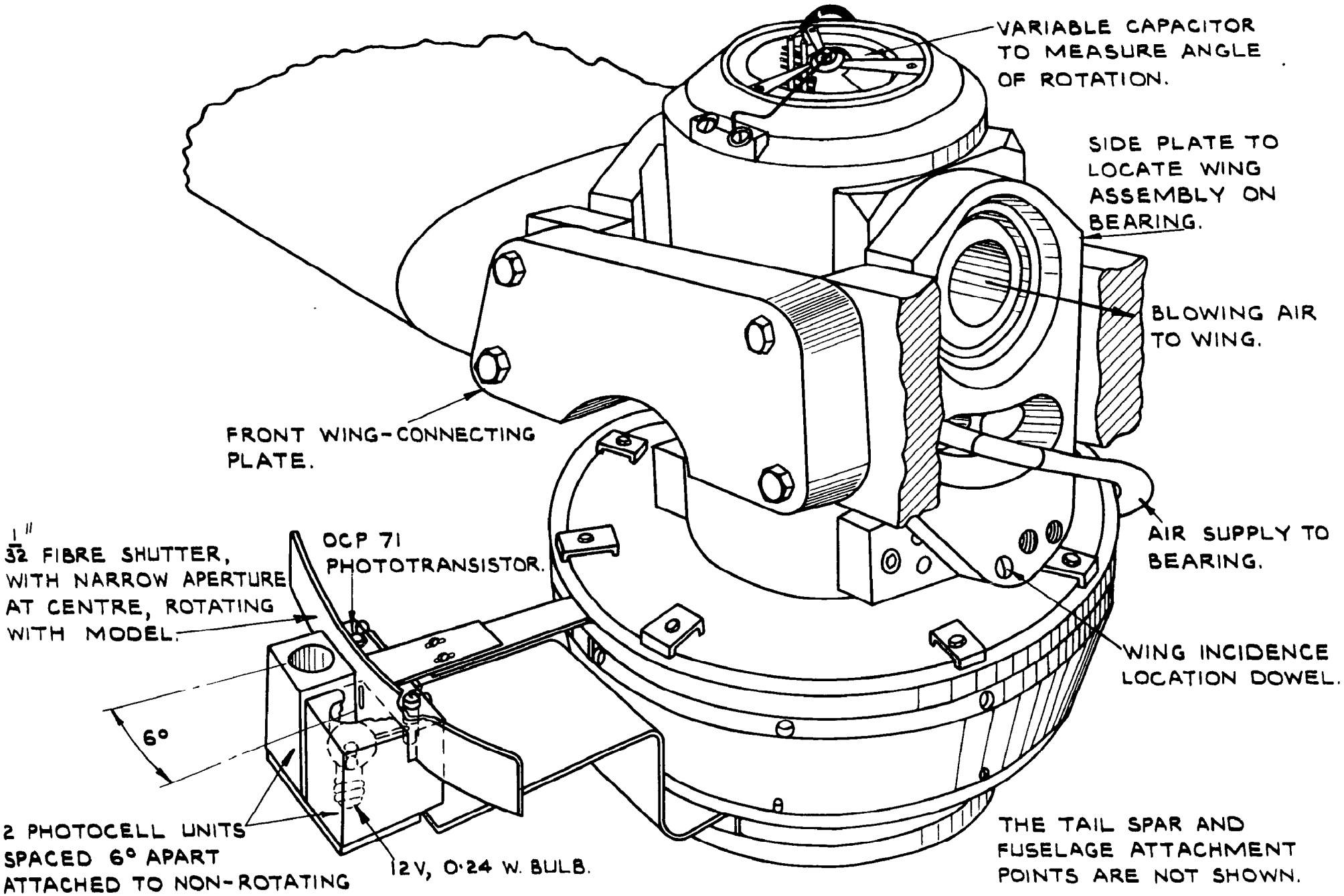

FIG. 3. DETAILS OF AIR-BEARING INSTALLATION AND AUTOMATIC CALIBRATION EQUIPMENT.

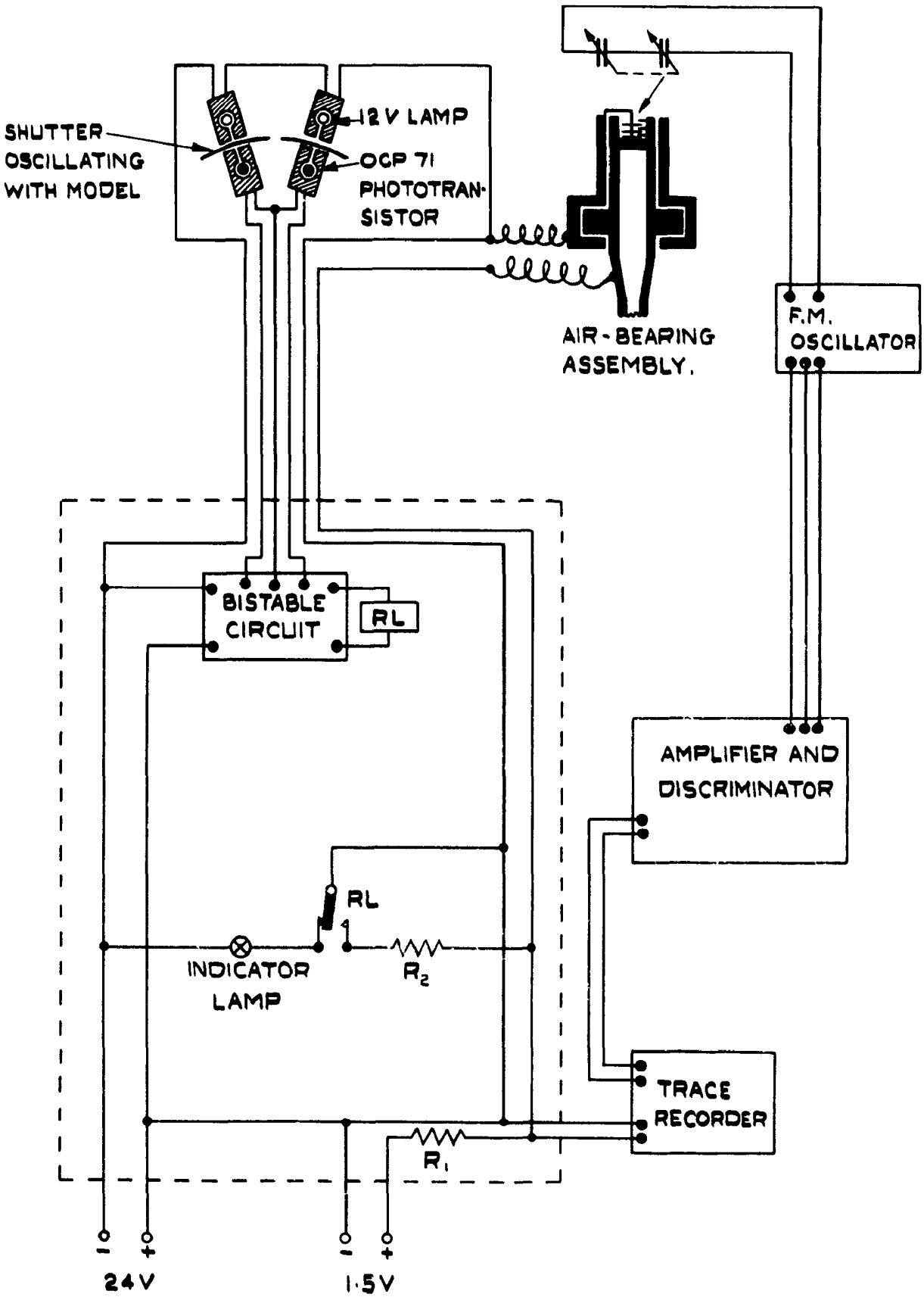

FIG. 4. CONNECTION OF APPARATUS.

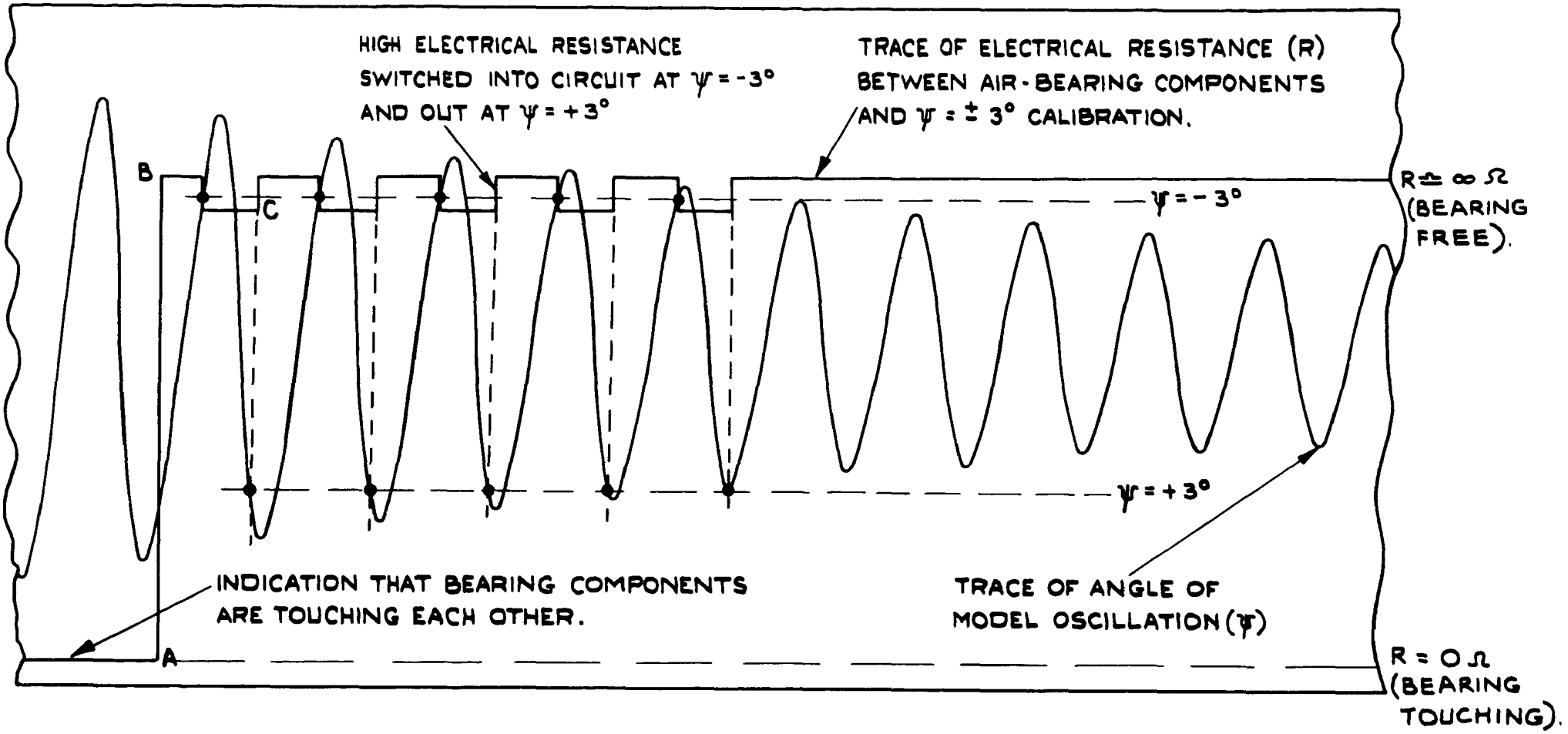

FIG. 5. PRESENTATION OF DATA ON TRACE RECORDS.

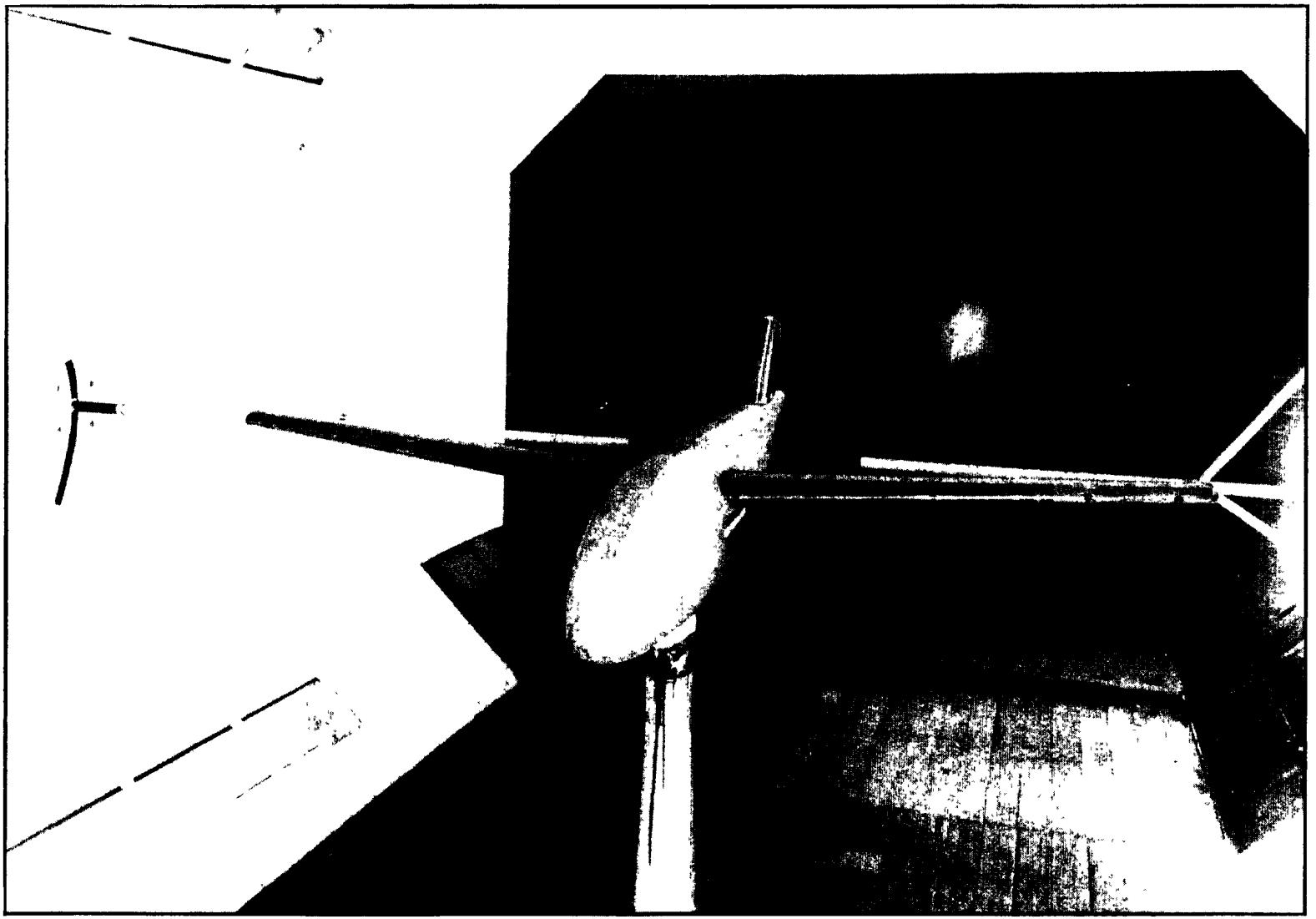

Fig.6 A.R.9. Jet-Flap model in the R.A.E. No.1 11½ft wind tunnel

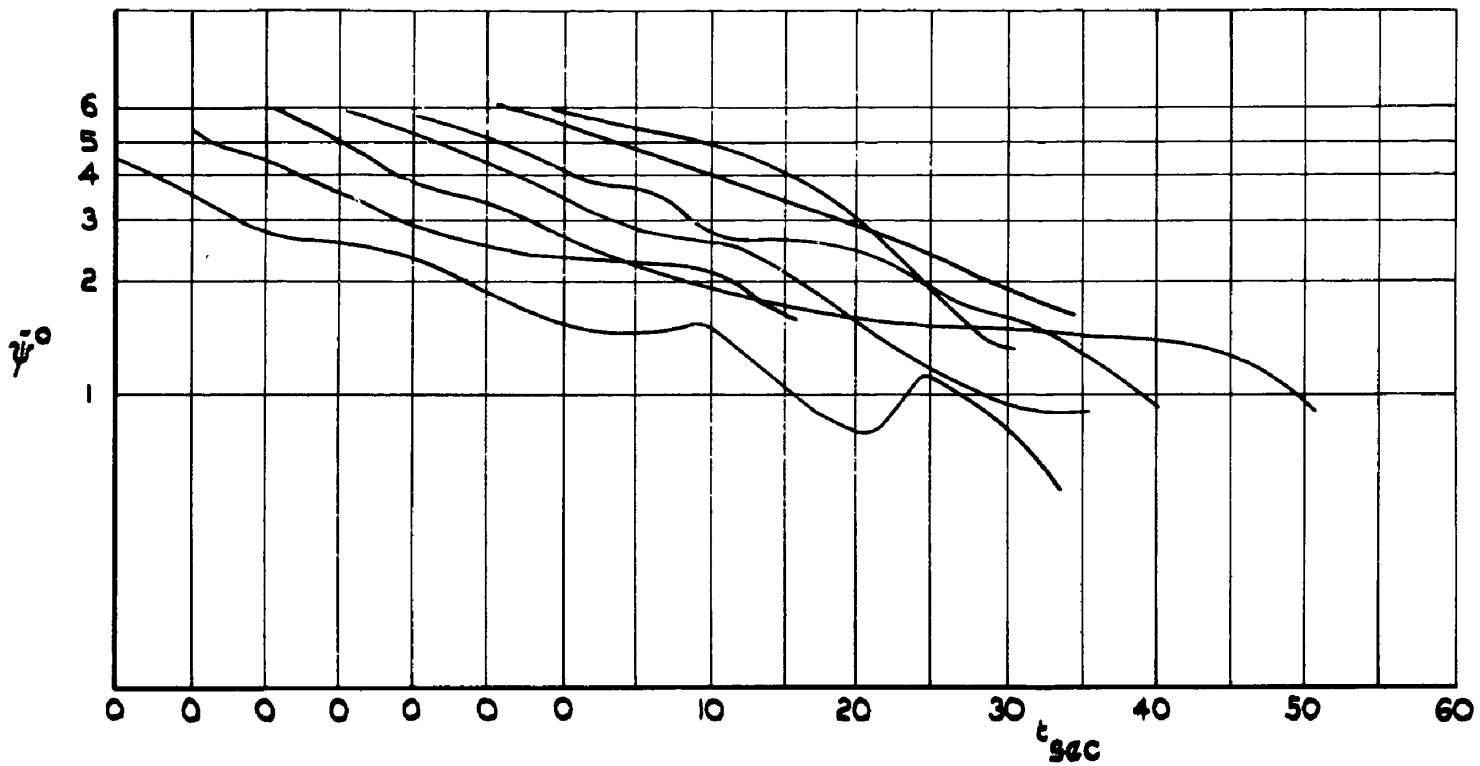

FIG. 7. COMPARISON OF SEVERAL TRACES WITH IDENTICAL MODEL CONDITIONS. MODEL WITH FIN, NO TAILPLANE, $\alpha_w = 0°$. CONTROL ANGLE = 30°, $C_\mu = 2 \cdot 1$.

SYMBOL	TEST SERIES
⊙	1
×	2
——	3

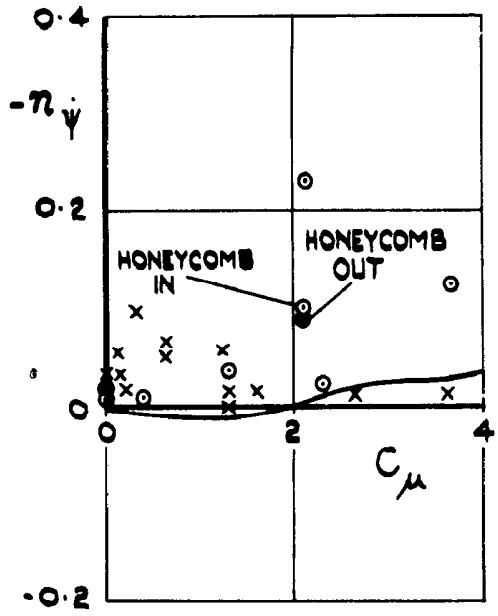

(a) $\alpha_w = 0°$; CONTROL ANGLE = 0° ($\theta \triangleq 20°$)

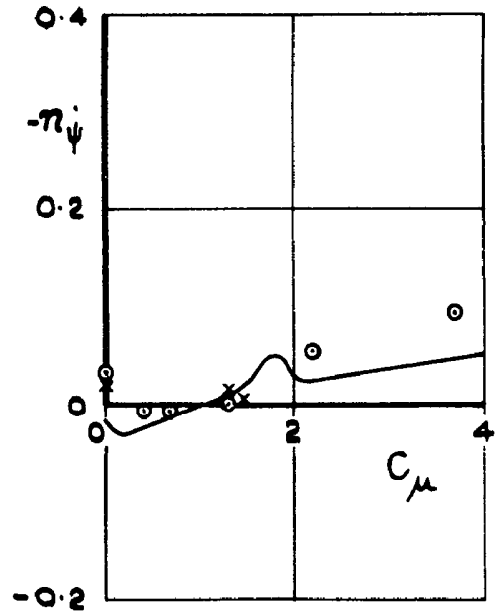

(b) $\alpha_w = 0°$; CONTROL ANGLE = 30° ($\theta \triangleq 50°$)

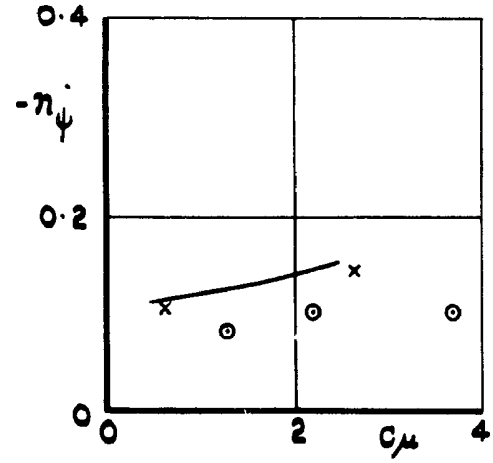

(c) $\alpha_w = 20°$; CONTROL ANGLE = 0° ($\theta \triangleq 20°$)

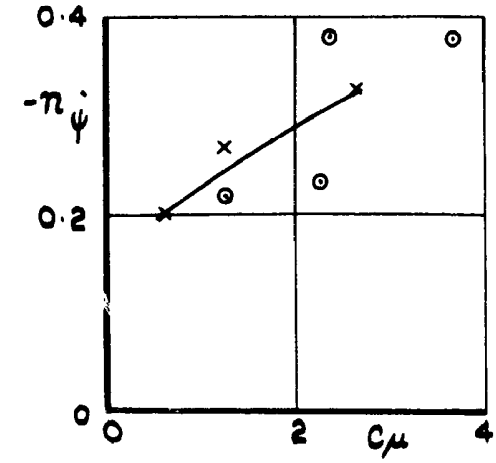

(d) $\alpha_w = 20°$; CONTROL ANGLE = 30° ($\theta \triangleq 50°$)

FIG. 8. COMPARISON OF PRELIMINARY AND MAIN TEST RESULTS. FIN OFF; $T_{NOM} = 2$ sec

SYMBOL	T_{sec}	ω_{nom}
+	1	0·197
△	2	0·140
×	3	0·070

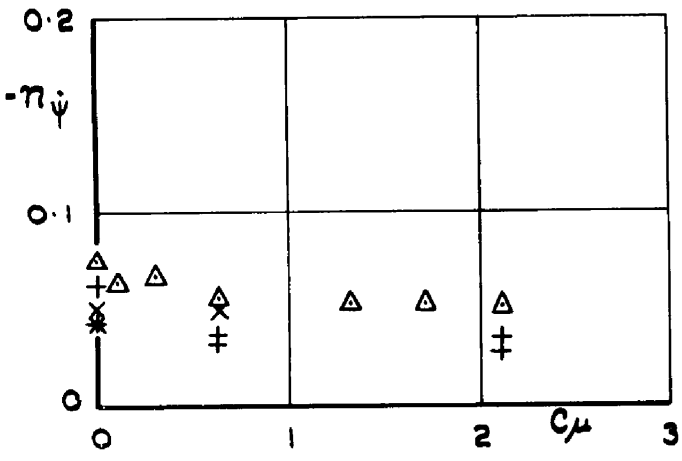

(a) α_W = 0°; CONTROL ANGLE = 0° ($\theta \triangleq 20°$)

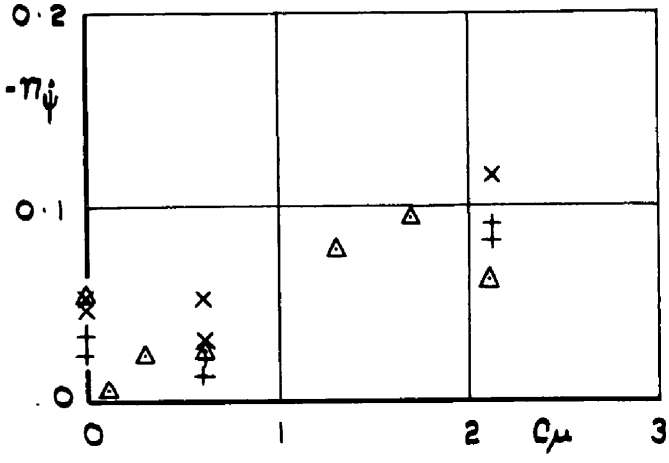

(b) α_W = 0°; CONTROL ANGLE = 30° ($\theta \triangleq 50°$)

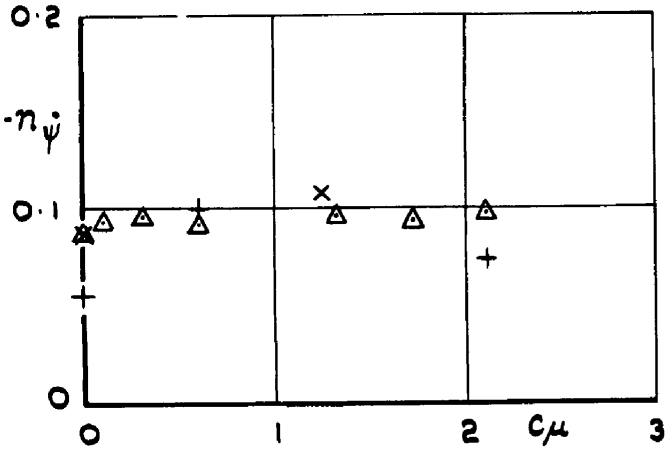

(c) α_W = 20°; CONTROL ANGLE = 0° ($\theta \triangleq 20°$)

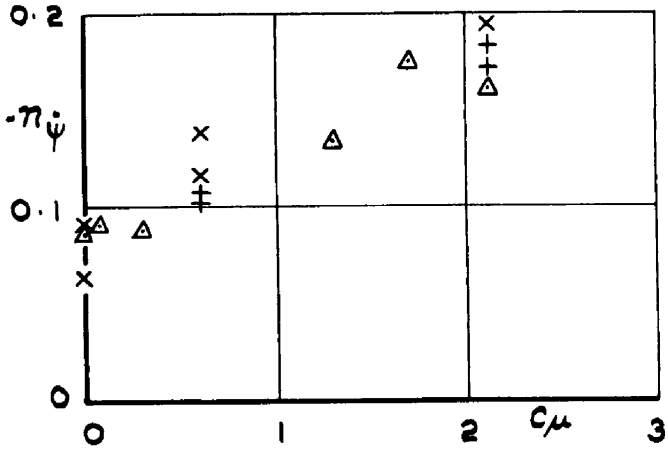

(d) α_W = 20°; CONTROL ANGLE = 30° ($\theta \triangleq 50°$)

FIG. 9. EFFECT OF FREQUENCY PARAMETER ON $n_{\dot{\psi}}$ v C_μ
V_o = 70 f.p.s.; FIN ON.

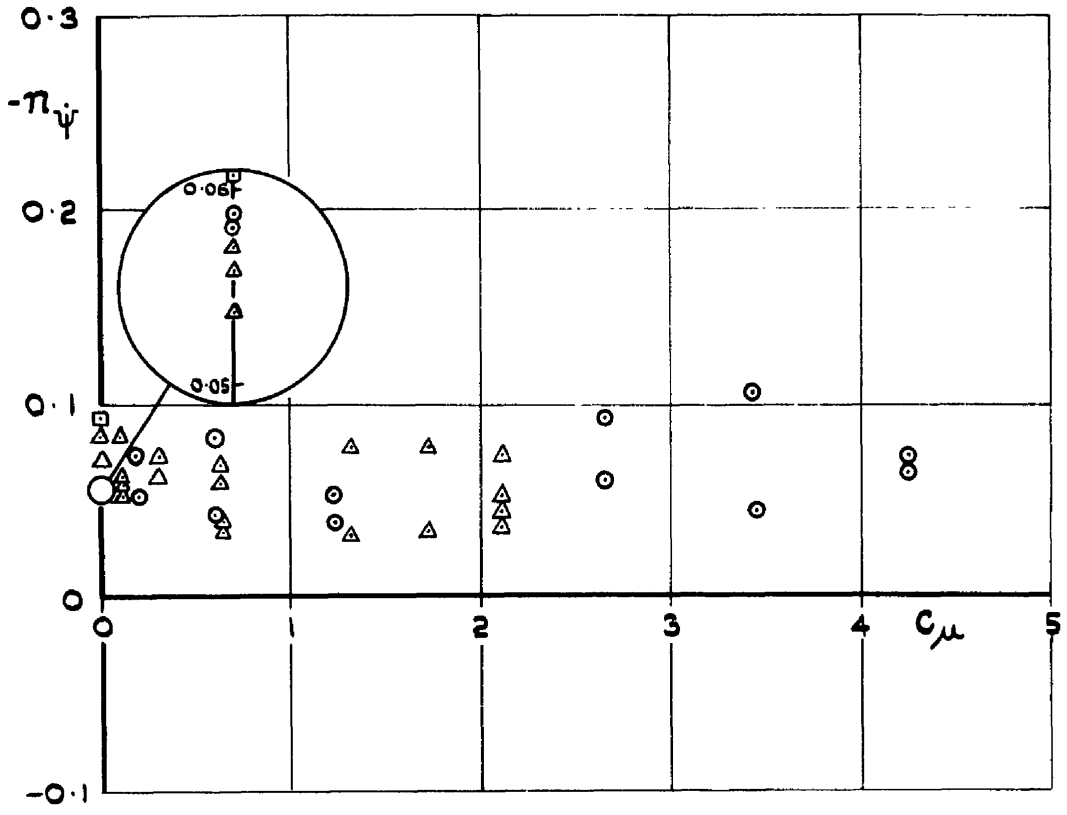

FIN ON, NO TAILPLANE.

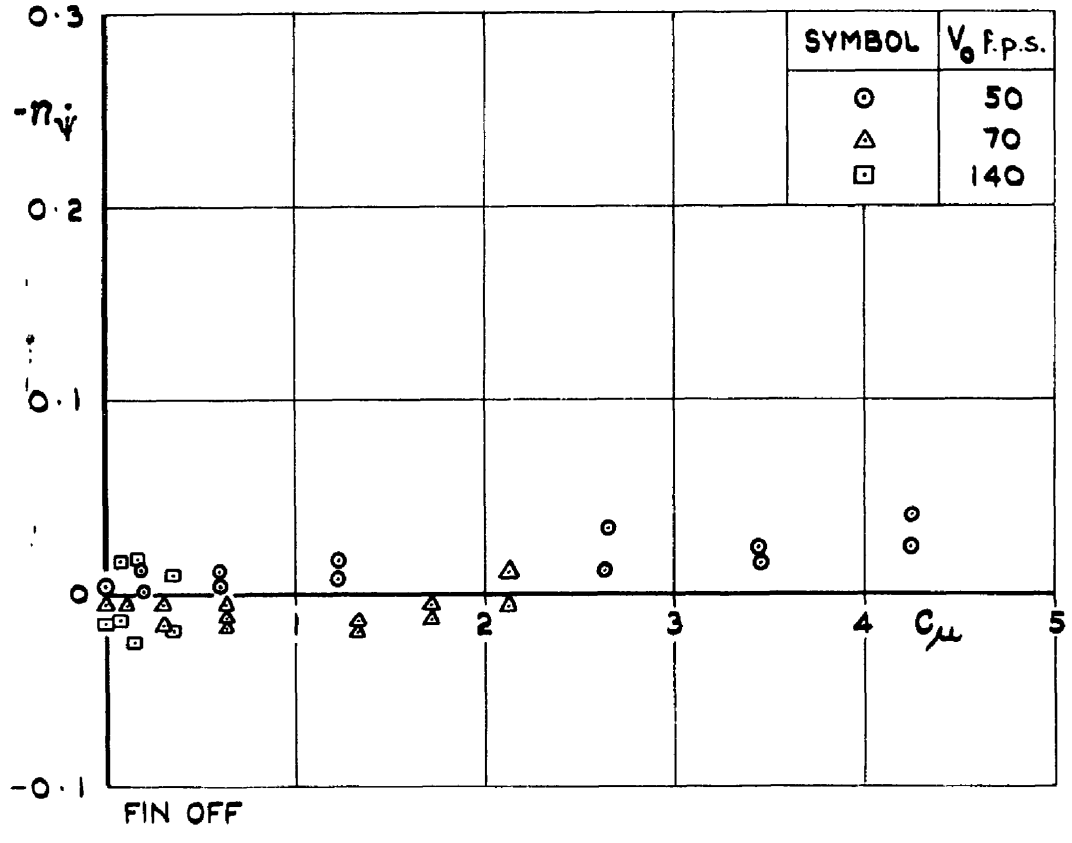

FIN OFF

(a) CONTROL ANGLE = 0° ($\theta \simeq 20°$).

FIG. 10. EFFECT OF C_μ ON $n_{\dot{\psi}}$ AT $\mathcal{L}_W$ = 0°. T_{NOM} = 2sec

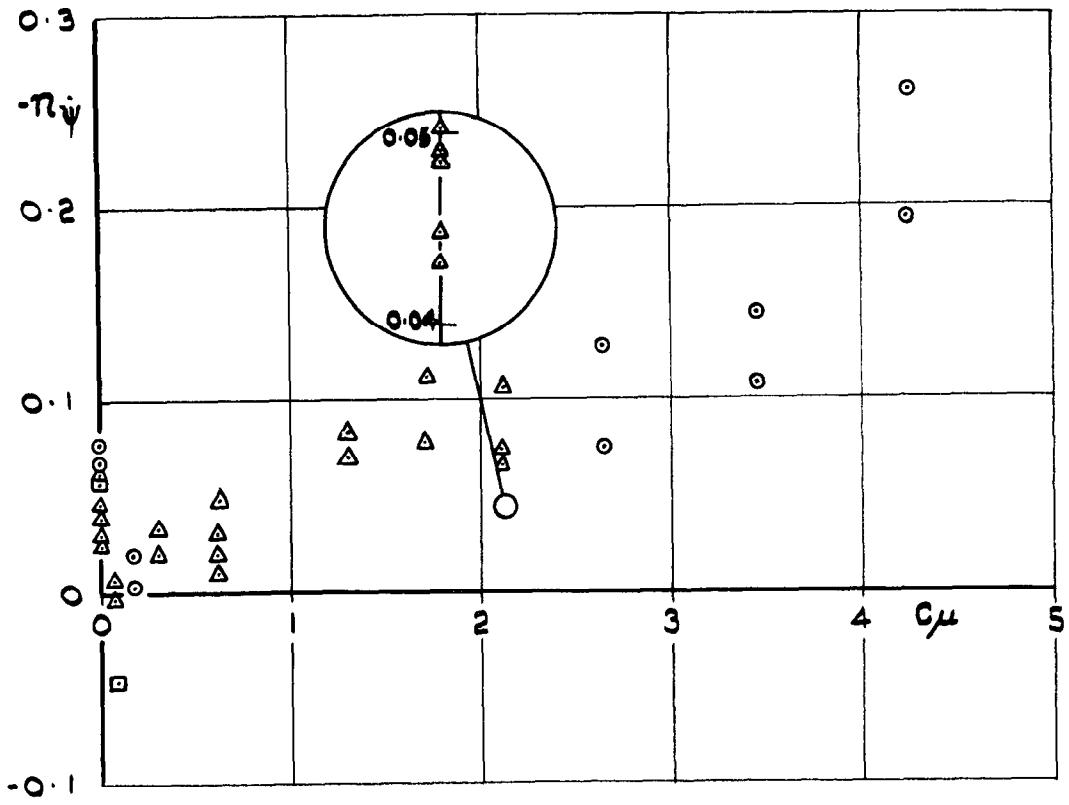

FIN ON, NO TAILPLANE

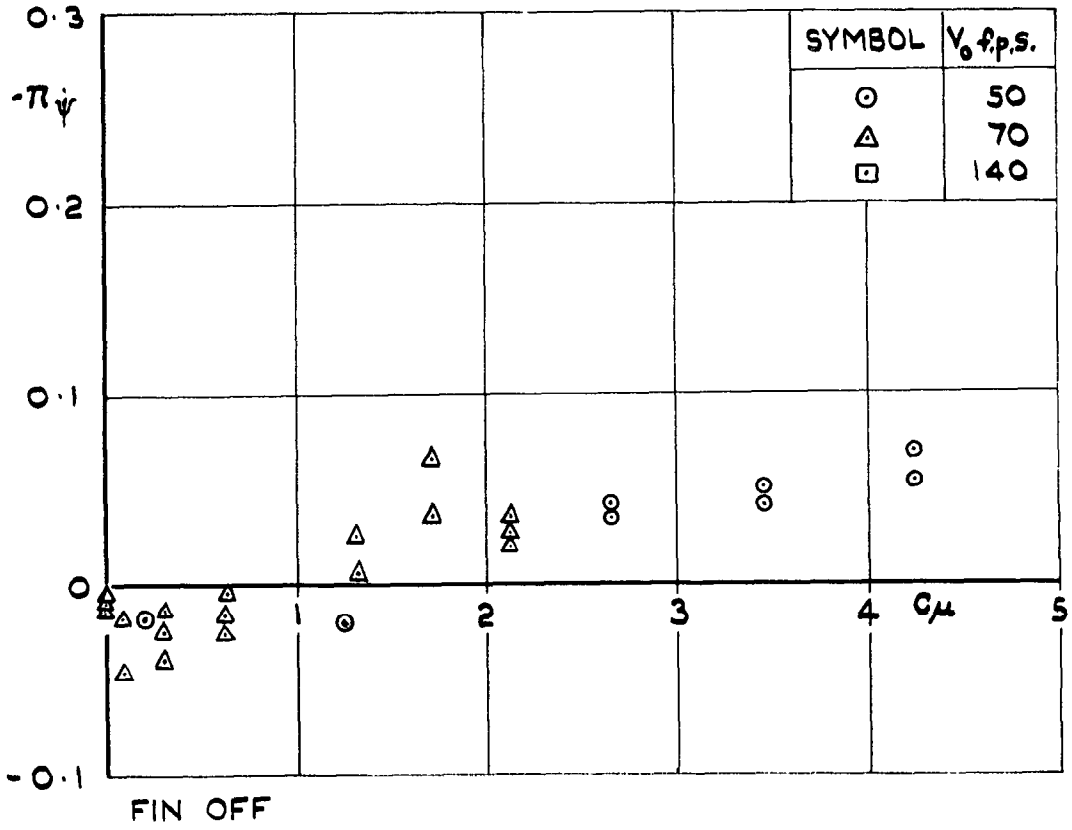

FIN OFF

(b) CONTROL ANGLE = 30° ($\theta \doteq 50°$)

FIG. 10. (CONT'D) EFFECT OF C_μ ON $n_{\dot{\psi}}$ AT $\mathcal{L}_W = 0°$. T_{NOM} = 2sec

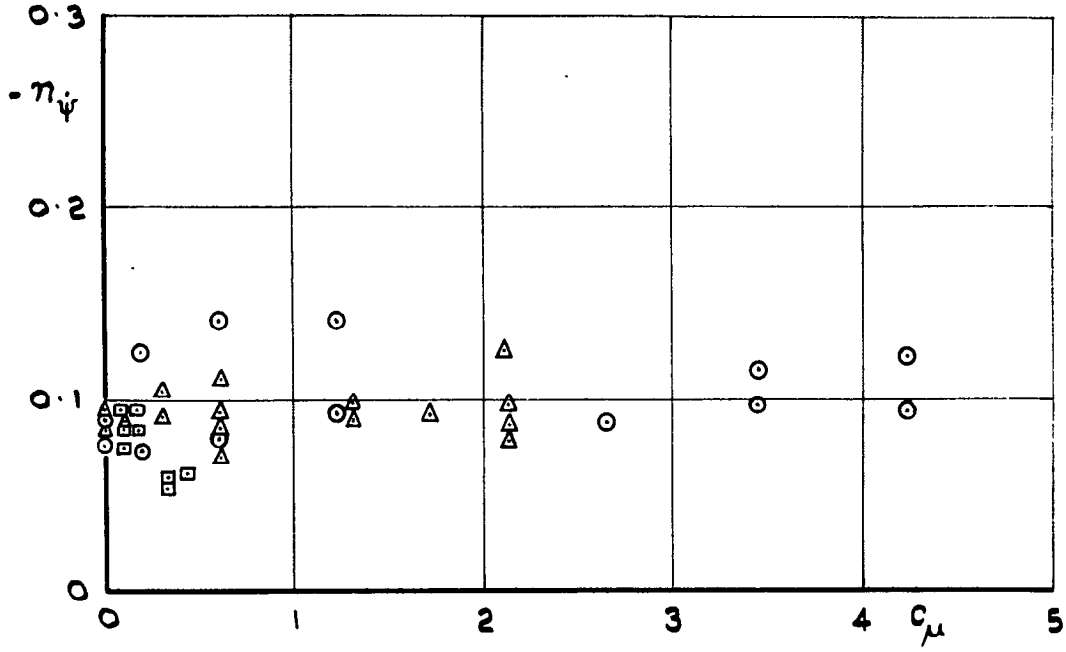

FIN ON, NO TAILPLANE

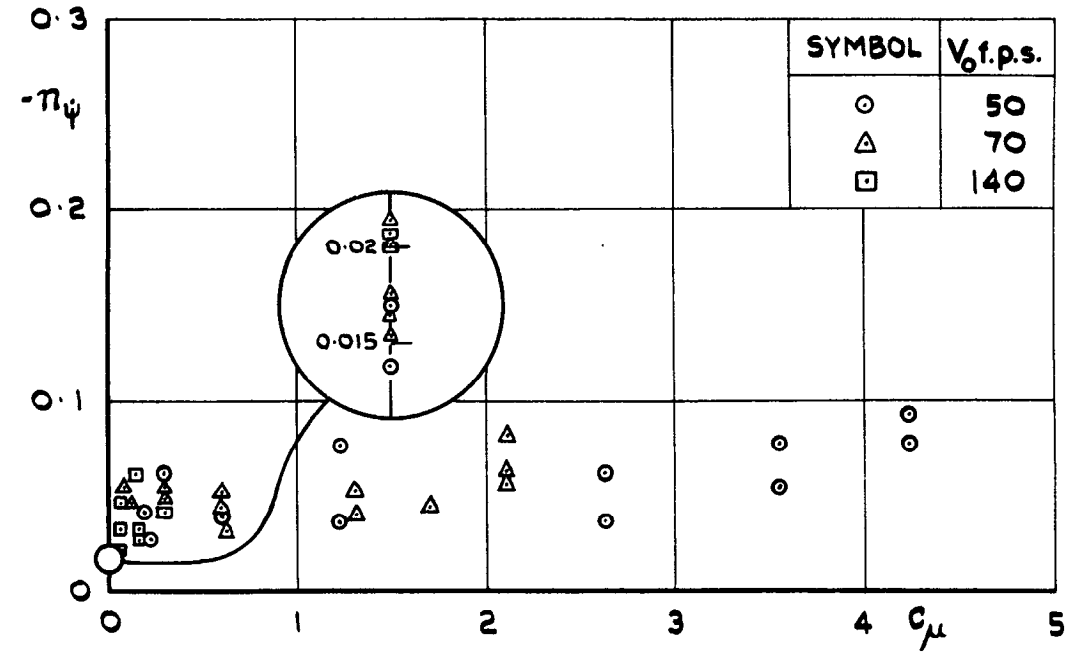

FIN OFF.

(a) CONTROL ANGLE = 0° ($\theta \doteq 20°$)

FIG. 11. EFFECT OF C_μ ON $n_{\dot{\psi}}$ AT $\alpha_w = 10°$. $T_{NOM} = 2$sec

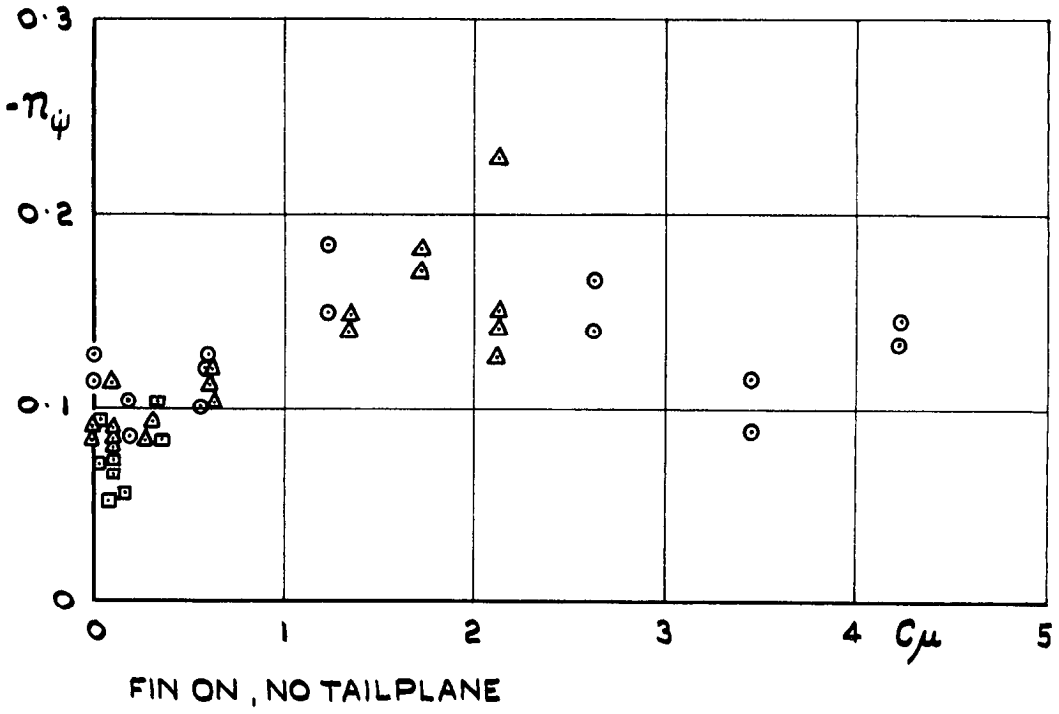

FIN ON, NO TAILPLANE

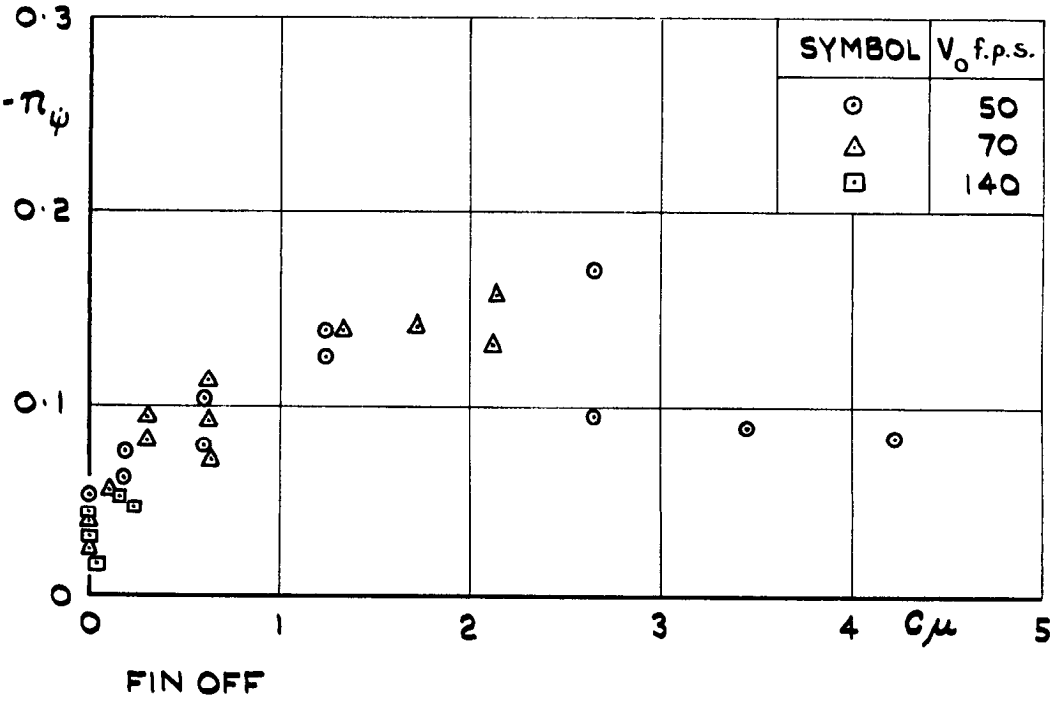

FIN OFF

(b) CONTROL ANGLE = 30° ($\theta \triangleq 50°$)

FIG. 11. (CONT'D) EFFECT OF C_μ ON η_ψ AT α_W = 10°. T_{NOM} = 2 sec.

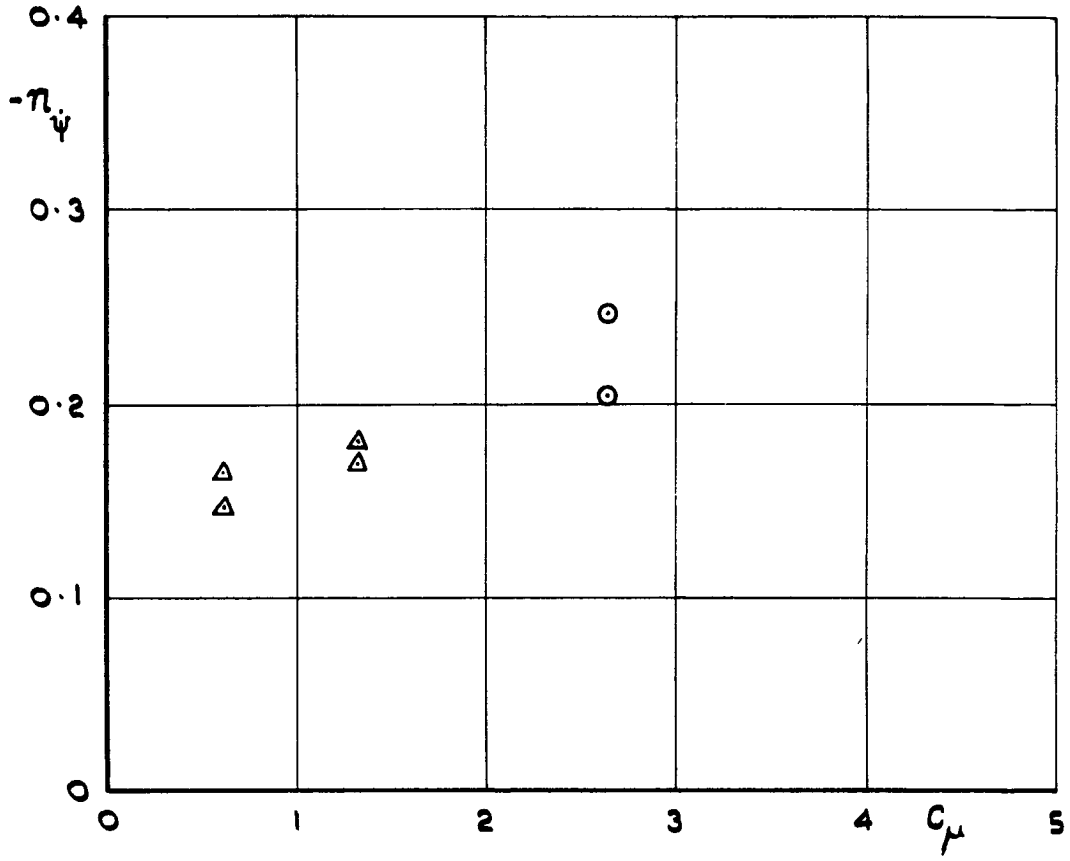

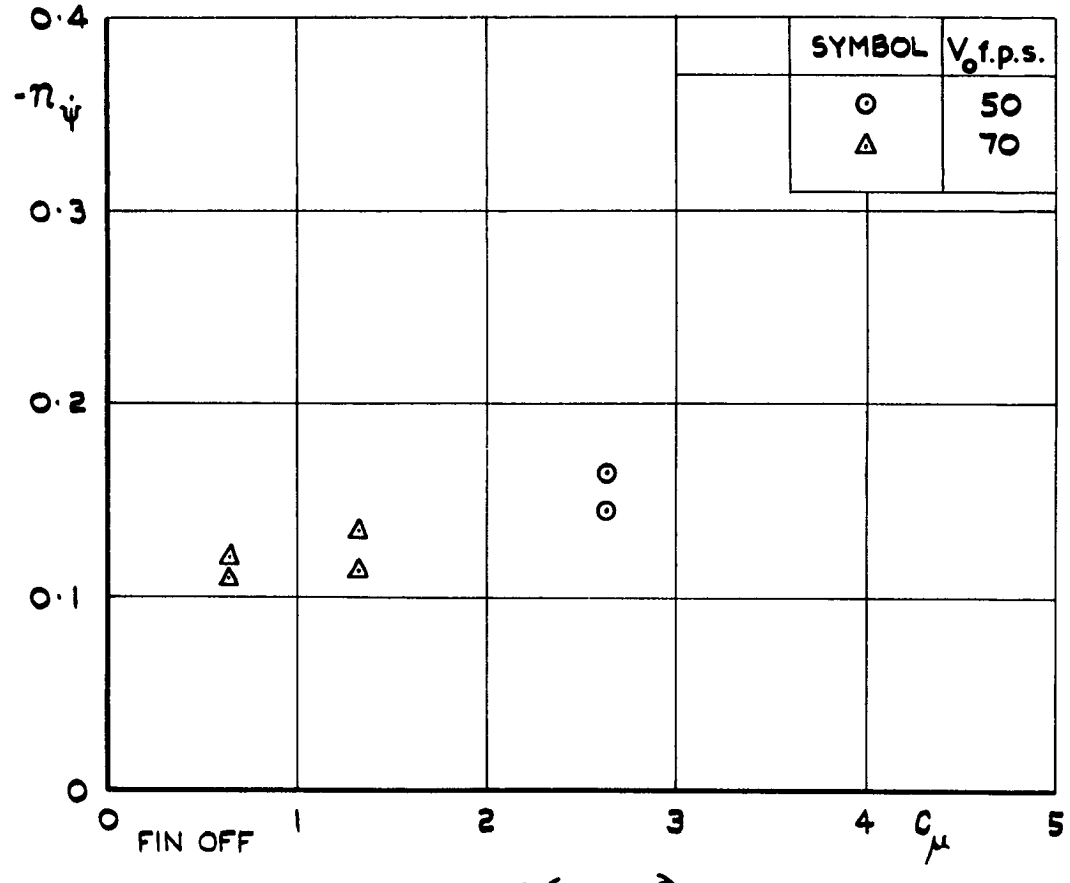

(a) CONTROL ANGLE = 0° ($\theta \simeq 20°$)

FIG. 12. EFFECT OF C_μ ON $n_{\dot{\psi}}$ AT α_w = 20° T_{NOM} = 2 sec.

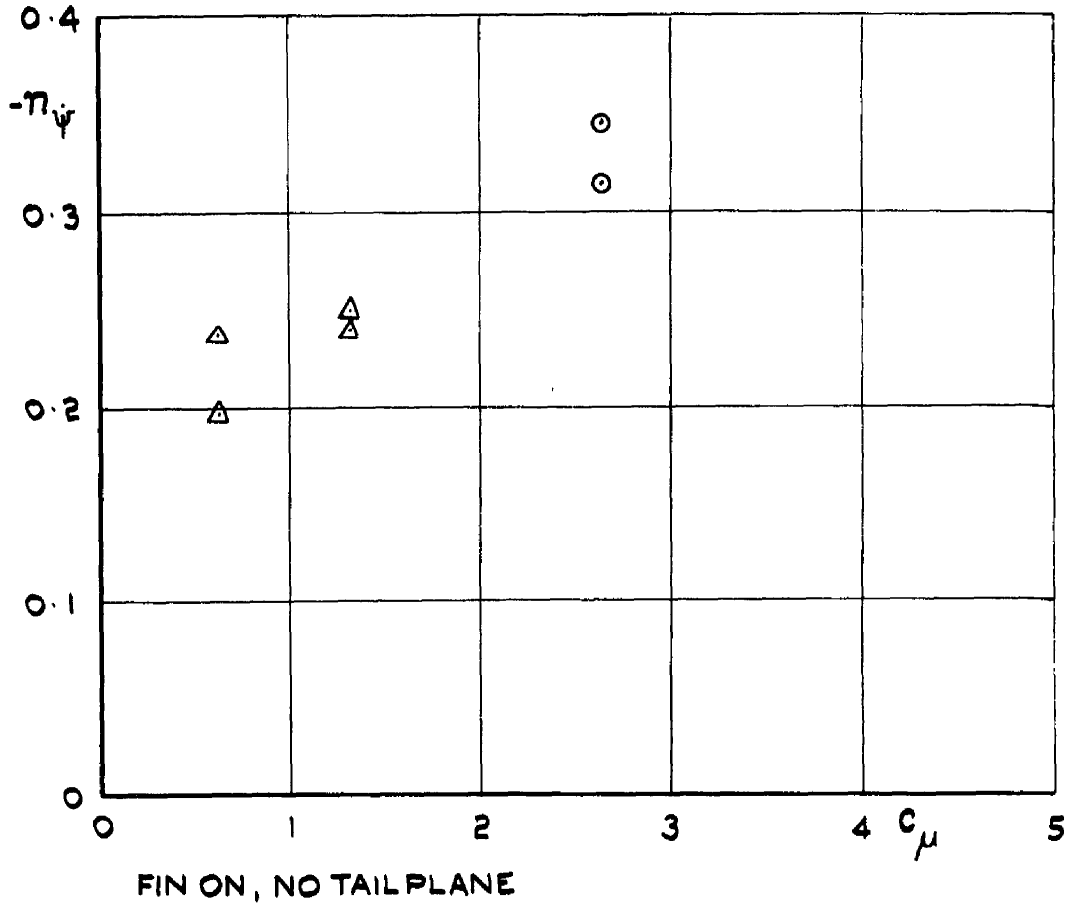

FIN ON, NO TAIL PLANE

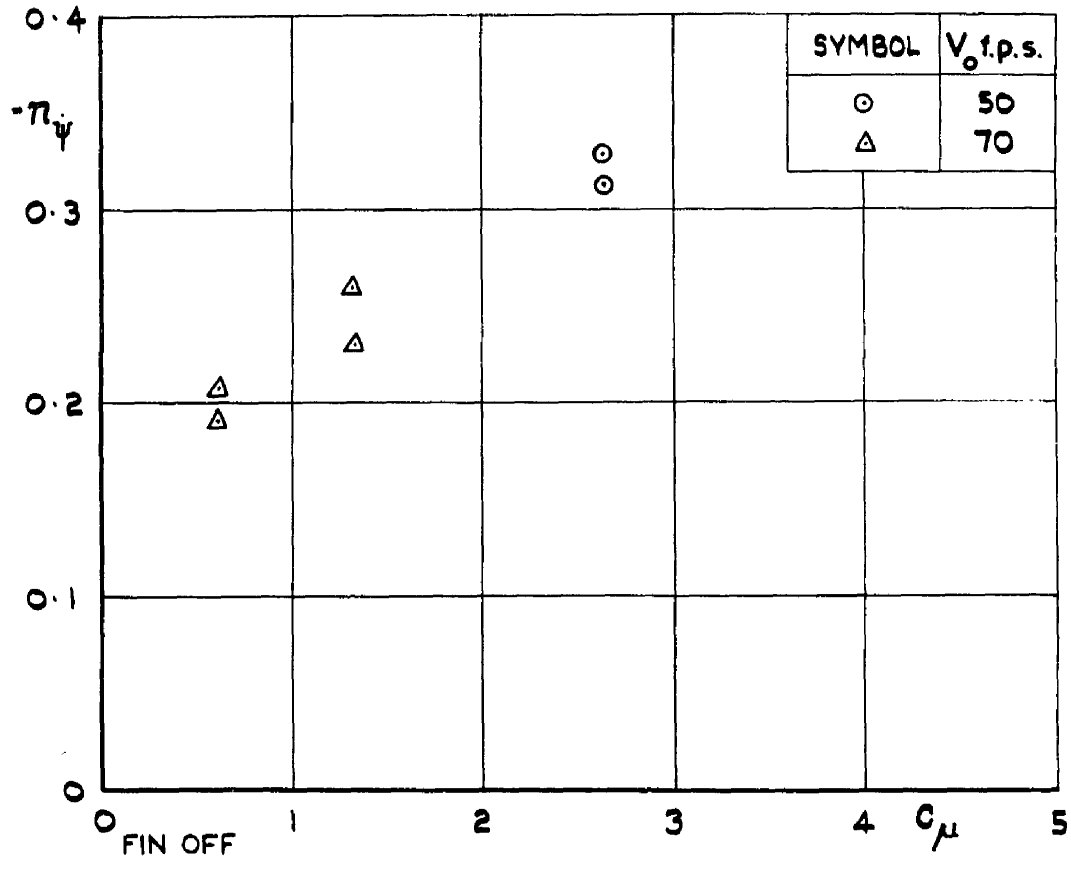

(b) CONTROL ANGLE = 30° ($\theta \triangleq 50°$).

FIG. 12. (CONT'D) EFFECT OF C_μ ON $n_{\dot{\psi}}$ AT $\mathcal{L}_W = 20°$. $T_{NOM.} = 2$ sec

SYMBOL	CONDITION
⊙	NO FIN
△	FIN ON, NO TAILPLANE
×	FIN AND TAILPLANE ON

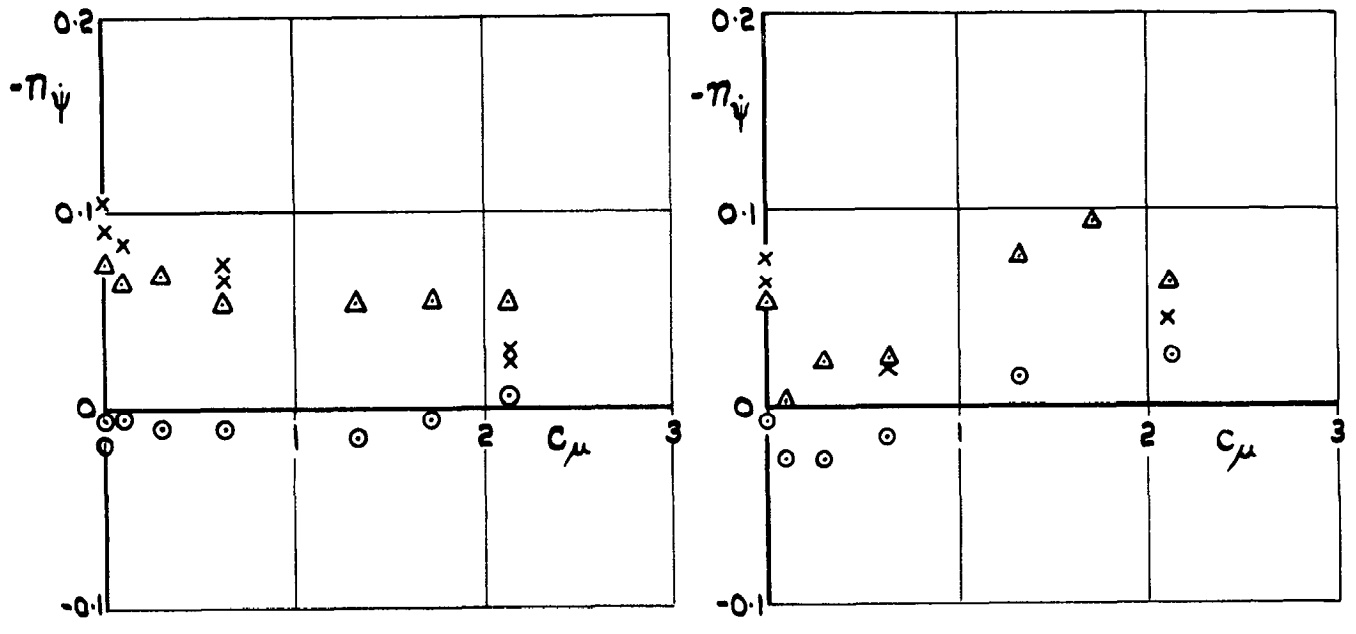

(a) $\alpha_w = 0°$; CONTROL ANGLE = 0° ($\theta \simeq 20°$) (b) $\alpha_w = 0°$; CONTROL ANGLE = 30° ($\theta \simeq 50°$)

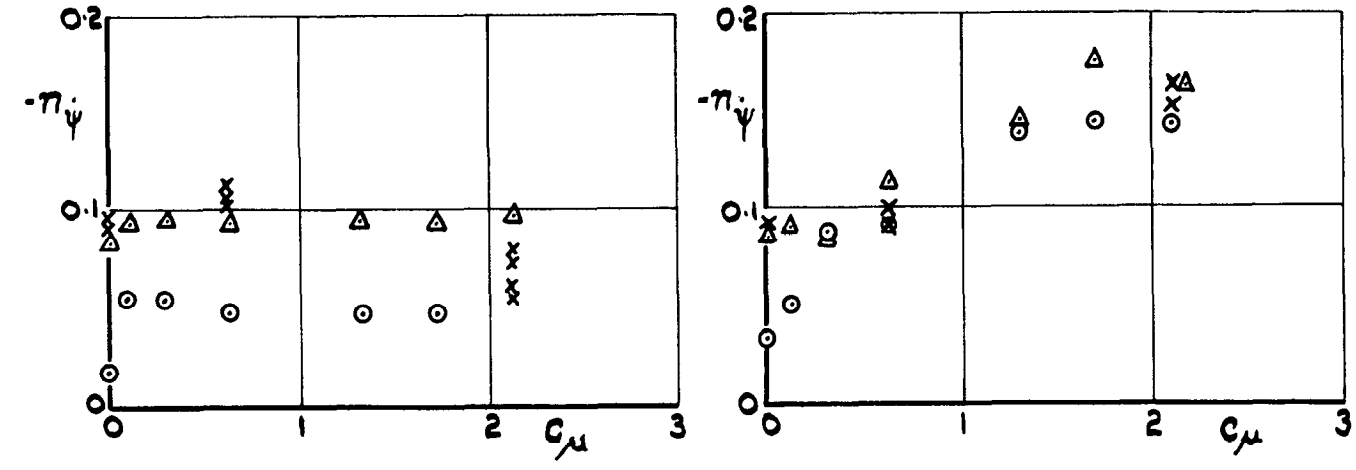

(c) $\alpha_w = 10°$; CONTROL ANGLE 0° ($\theta \simeq 20°$) (d) $\alpha_w = 10°$; CONTROL ANGLE = 30° ($\theta \simeq 50°$)

FIG. 13. EFFECT OF TAILPLANE ON $n_{\dot{\psi}}$ v C_μ
$V_0 = 70$ f.p.s. $T_{NOM.} = 2$ sec. $\Delta C_{L_{TAIL}} \simeq 0$.

SYMBOL	CONDITION
△	BASIC MODEL
×	BASIC MODEL + FUSELAGE SPOILER
+	BASIC MODEL + DORSAL FIN

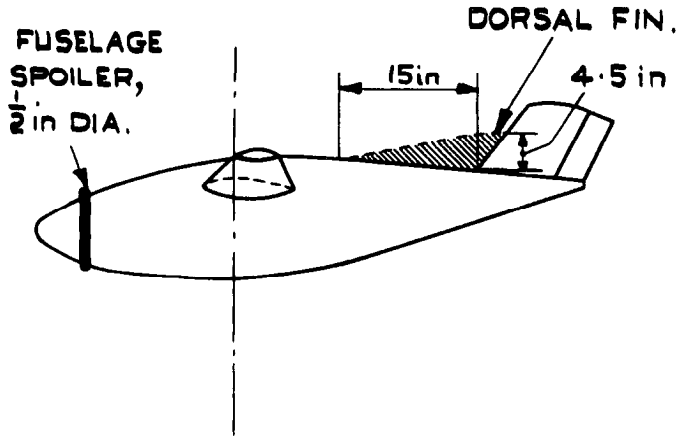

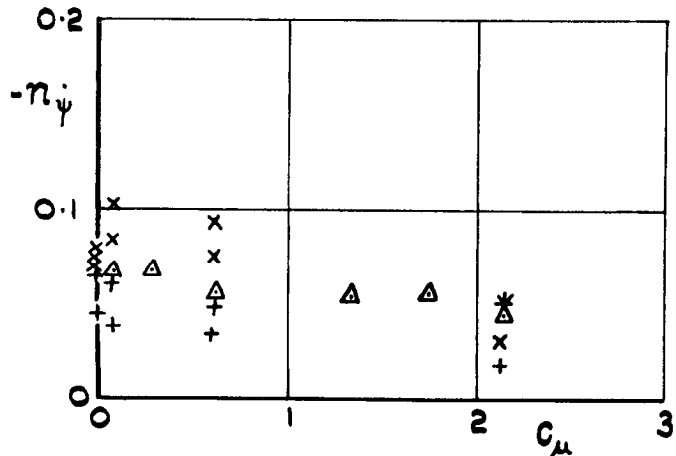

(a) CONTROL ANGLE = 0° (θ ≙ 20°).

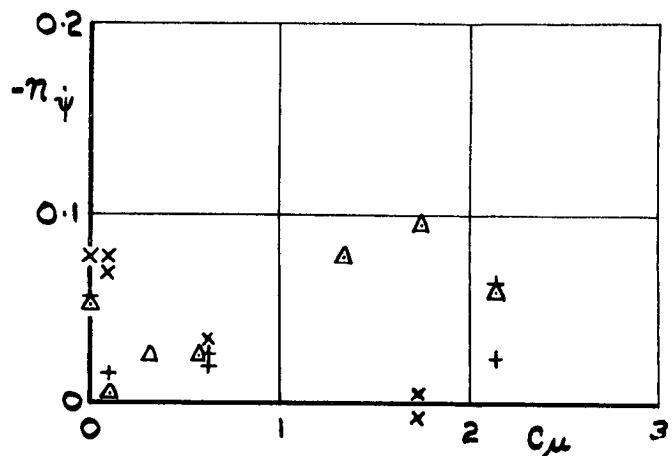

(b) CONTROL ANGLE = 30° (θ ≙ 50°)

FIG. 14. EFFECT OF DORSAL FIN AND FUSELAGE SPOILER ON $n_{\dot{\psi}}$ v C_μ

FIN ON, NO TAILPLANE, V_o = 70 f.p.s. $\mathcal{L}_W$ = 0°, T_{NOM} = 2 sec.

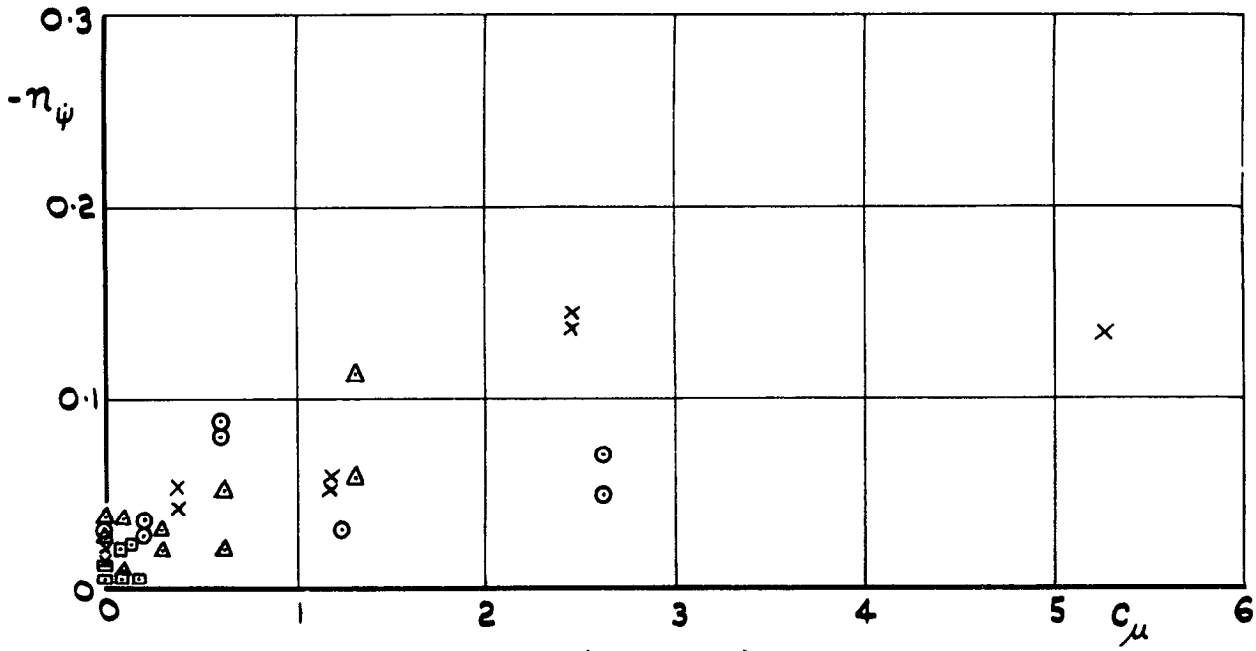

(a) CONTROL ANGLE = 0° ($\theta \triangleq 20°$)

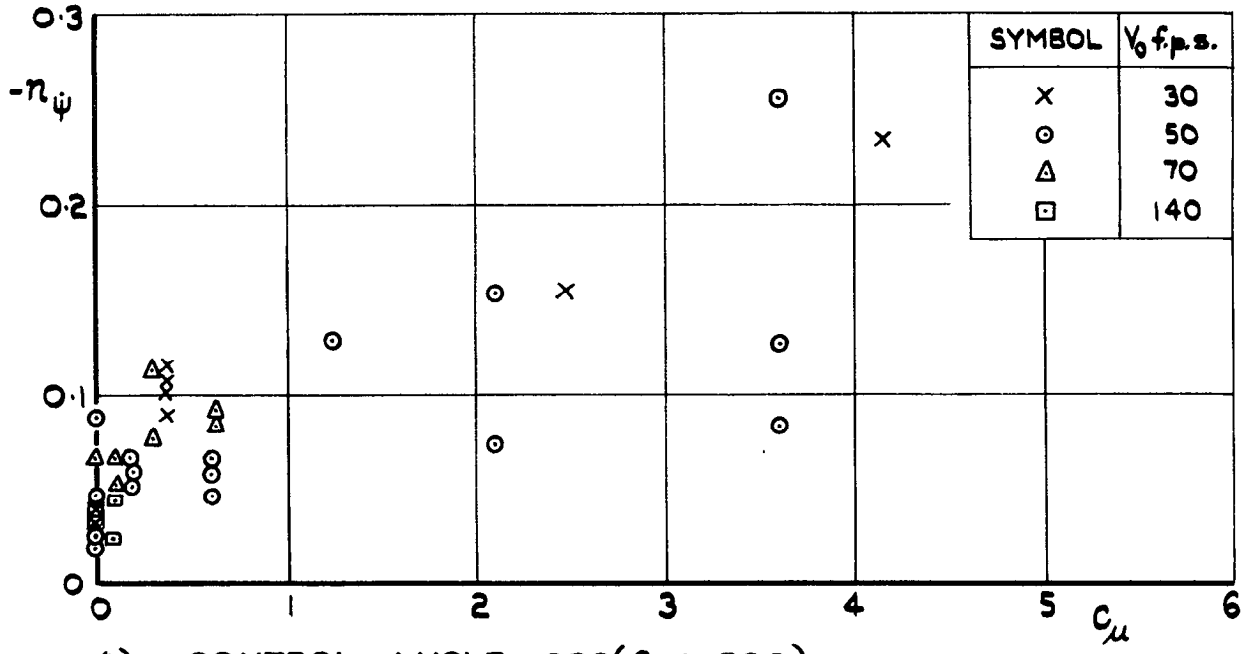

(b) CONTROL ANGLE = 30° ($\theta \triangleq 50°$)

FIG. 15. EFFECT OF C_{μ} ON n_{ψ} AT $\alpha_W = 0°$ FOR WING-ALONE MODEL (NO FUSELAGE.) $T_{NOM} = 4$ sec.

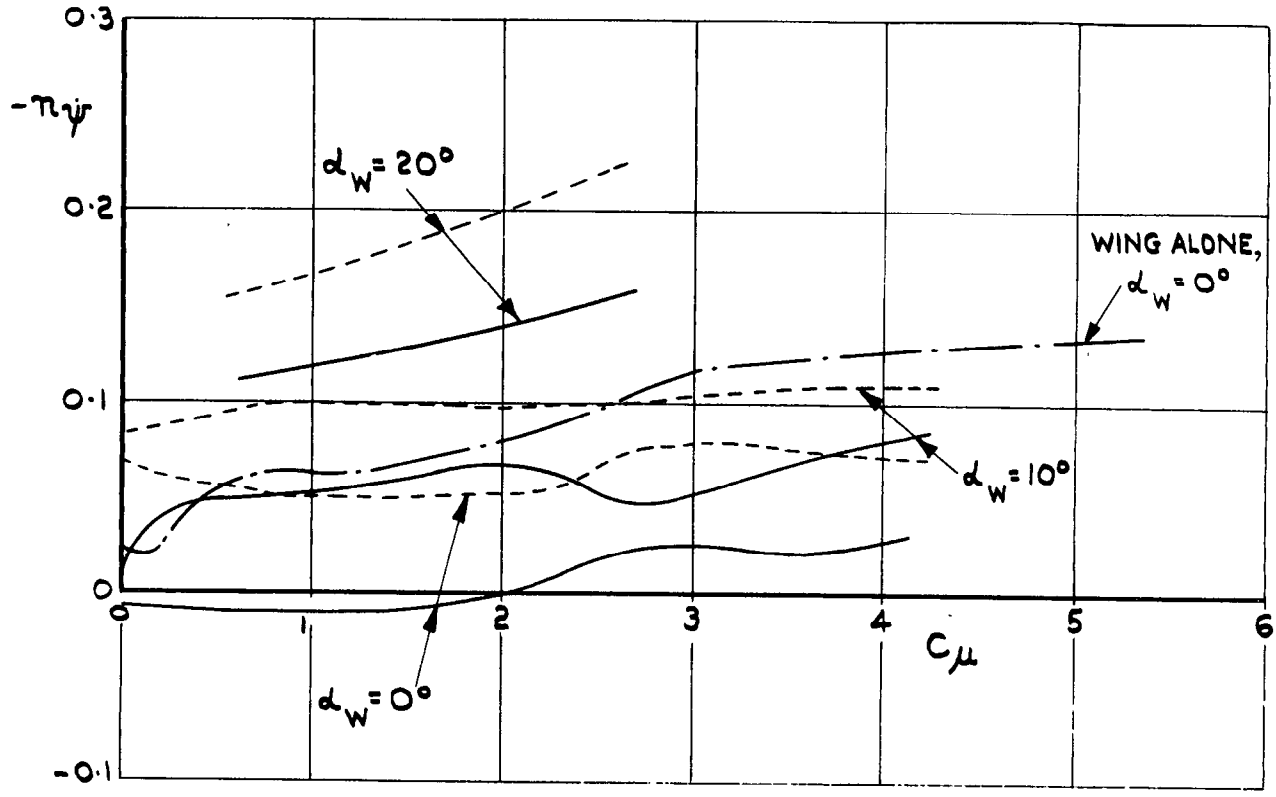

(a). CONTROL ANGLE = 0° ($\theta \simeq 20°$).

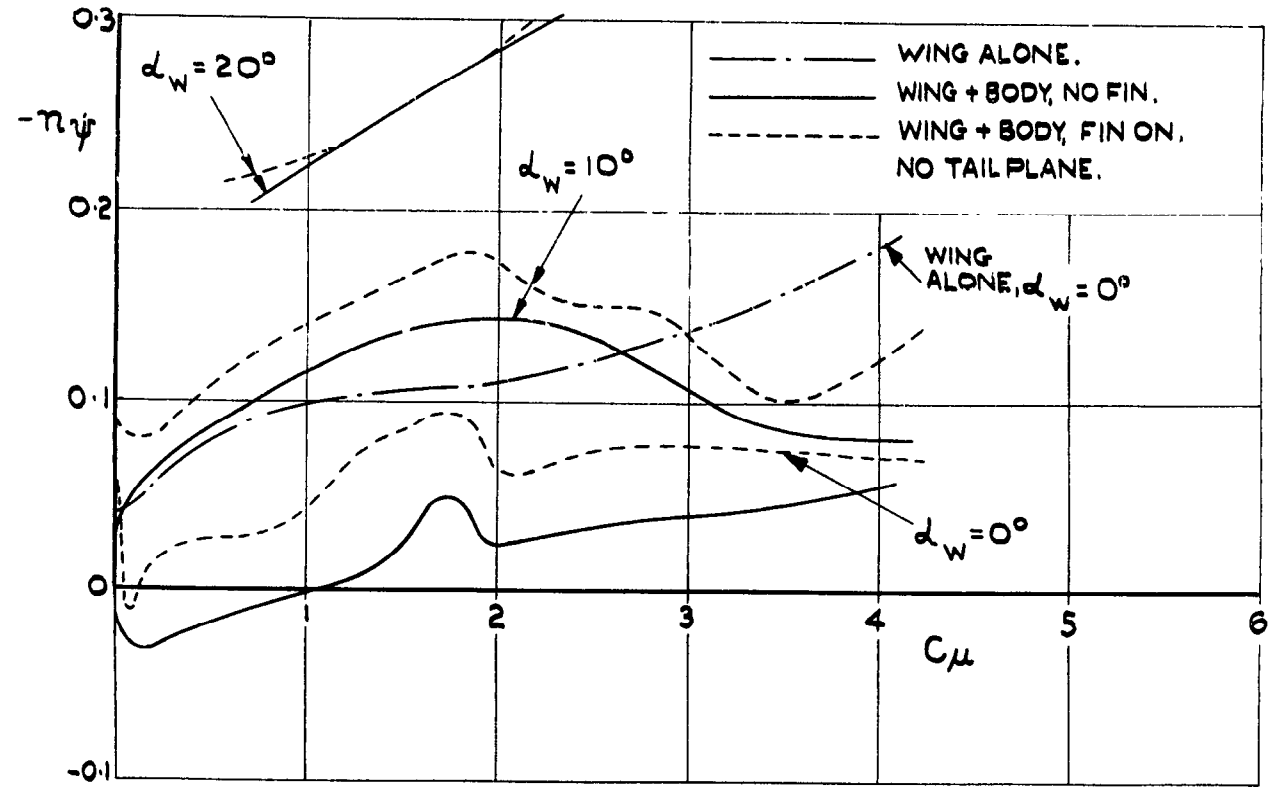

(b). CONTROL ANGLE = 30° ($\theta \simeq 50°$).

FIG. 16. EFFECT OF WING INCIDENCE AND FUSELAGE PRESENCE ON n_ψ v C_μ. $T_{NOM.}$ = 2 sec.

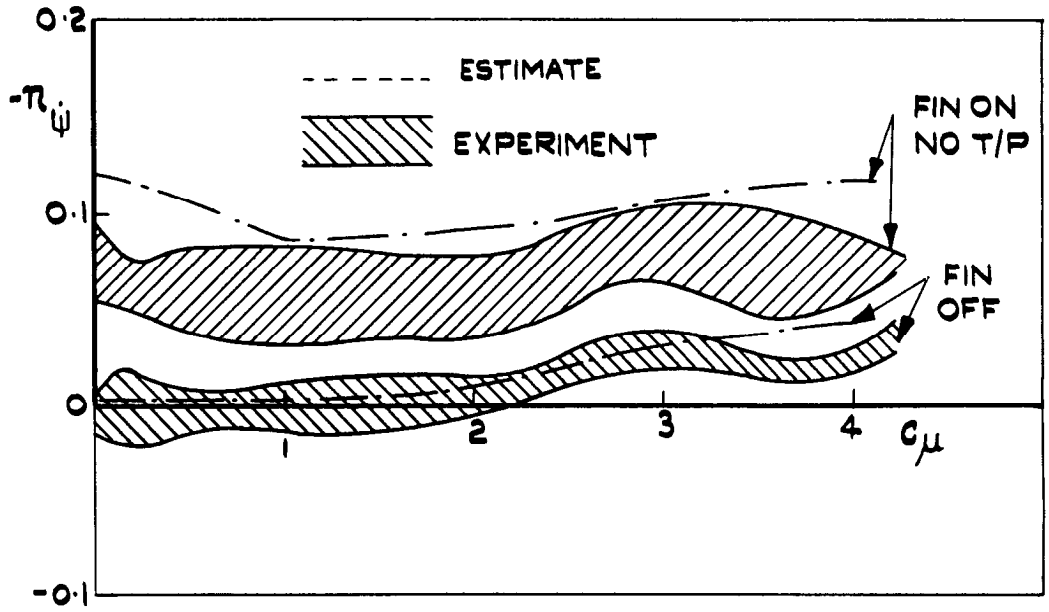

(a). CONTROL ANGLE = 0° ($\theta \triangleq 20°$).

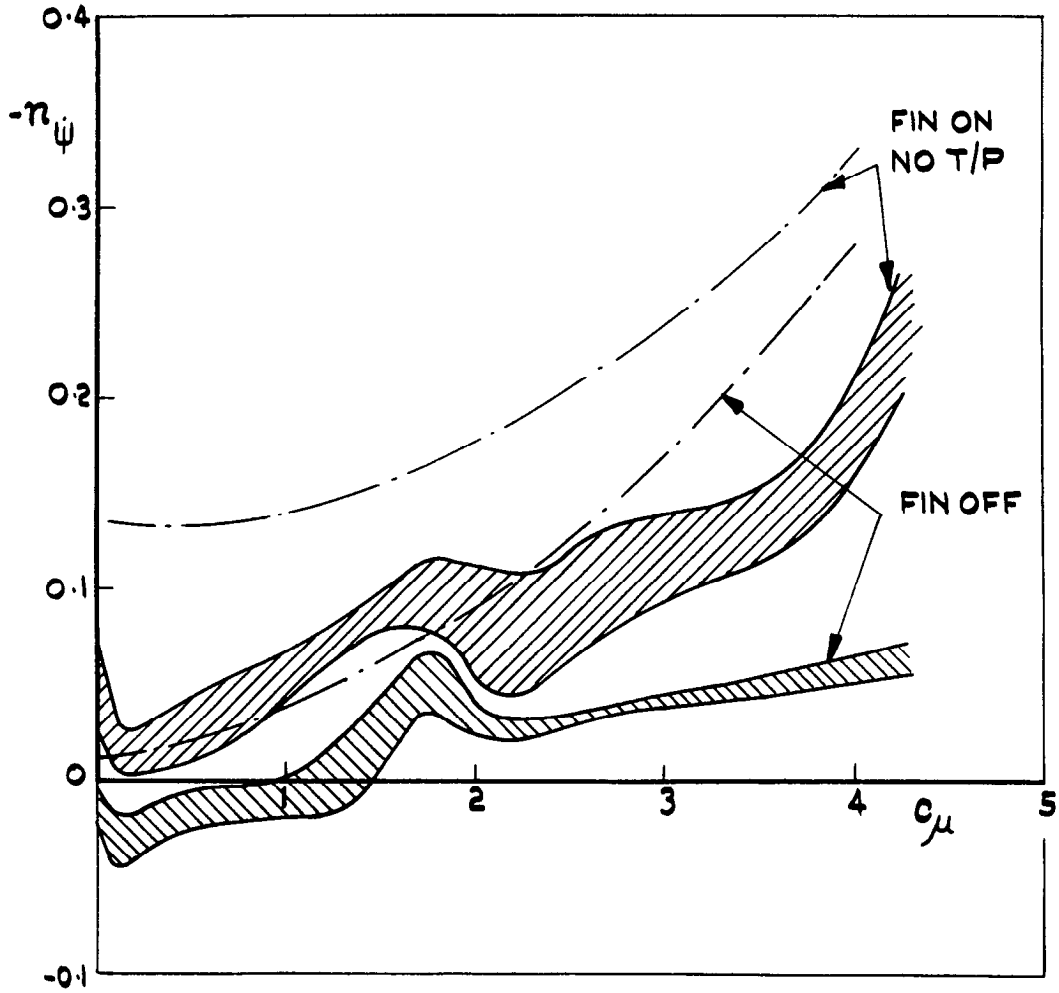

(b) CONTROL ANGLE = 30°($\theta \triangleq 50°$)

FIG 17 COMPARISON WITH ESTIMATES AT $\mathcal{L}_W$ = 0°, T_{NOM} = 2 sec.

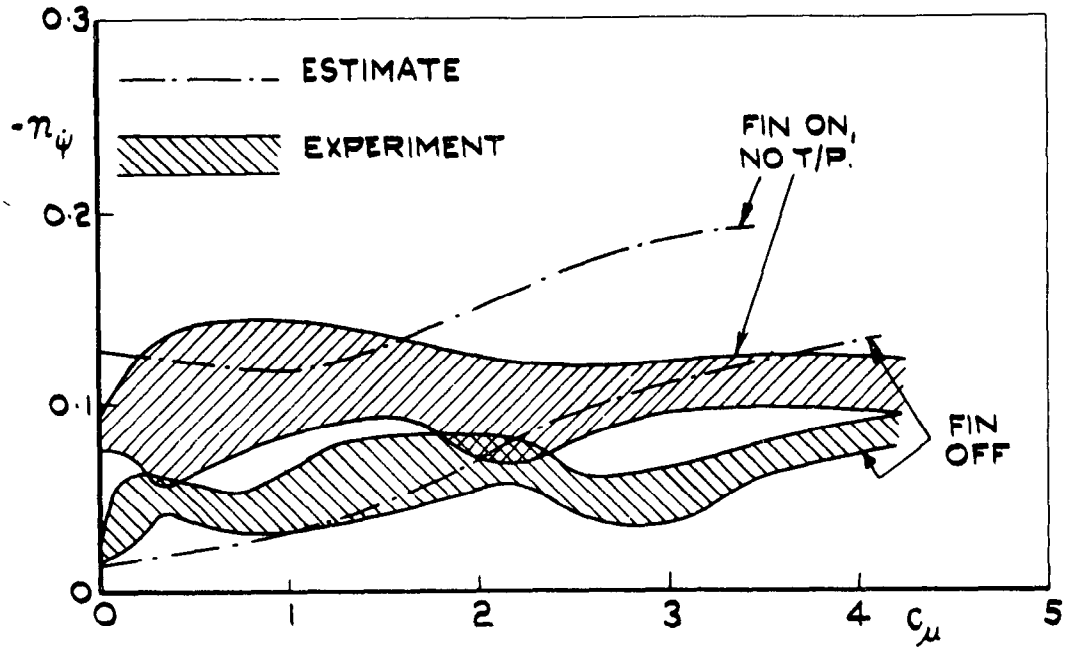

(a). CONTROL ANGLE = 0° ($\theta \simeq 20°$).

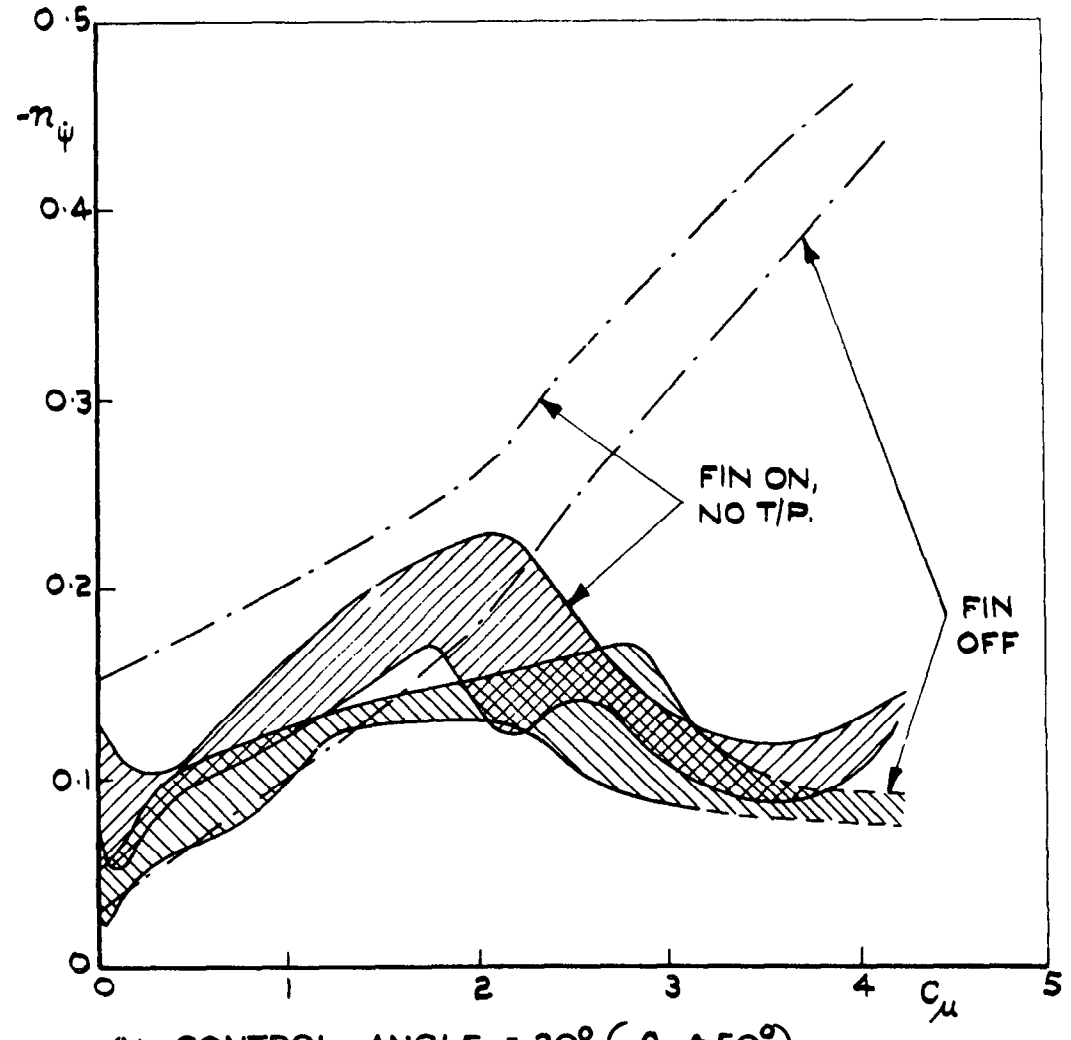

(b). CONTROL ANGLE = 30° ($\theta \simeq 50°$).

FIG. 18. COMPARISON WITH ESTIMATES AT $\alpha_W = 10°$, $T_{NOM.} = 2$ sec.

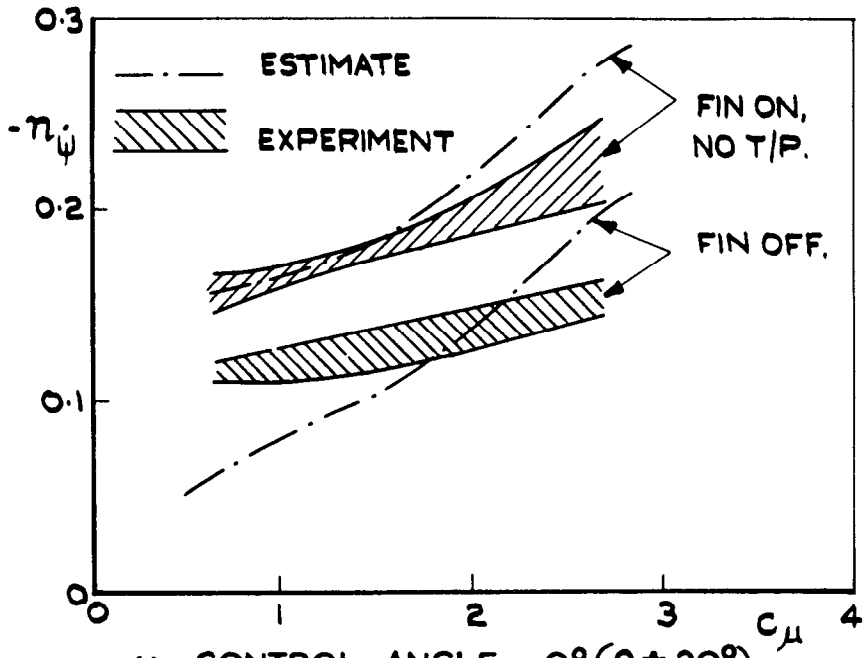

(a). CONTROL ANGLE = 0° ($\theta \triangleq 20°$).

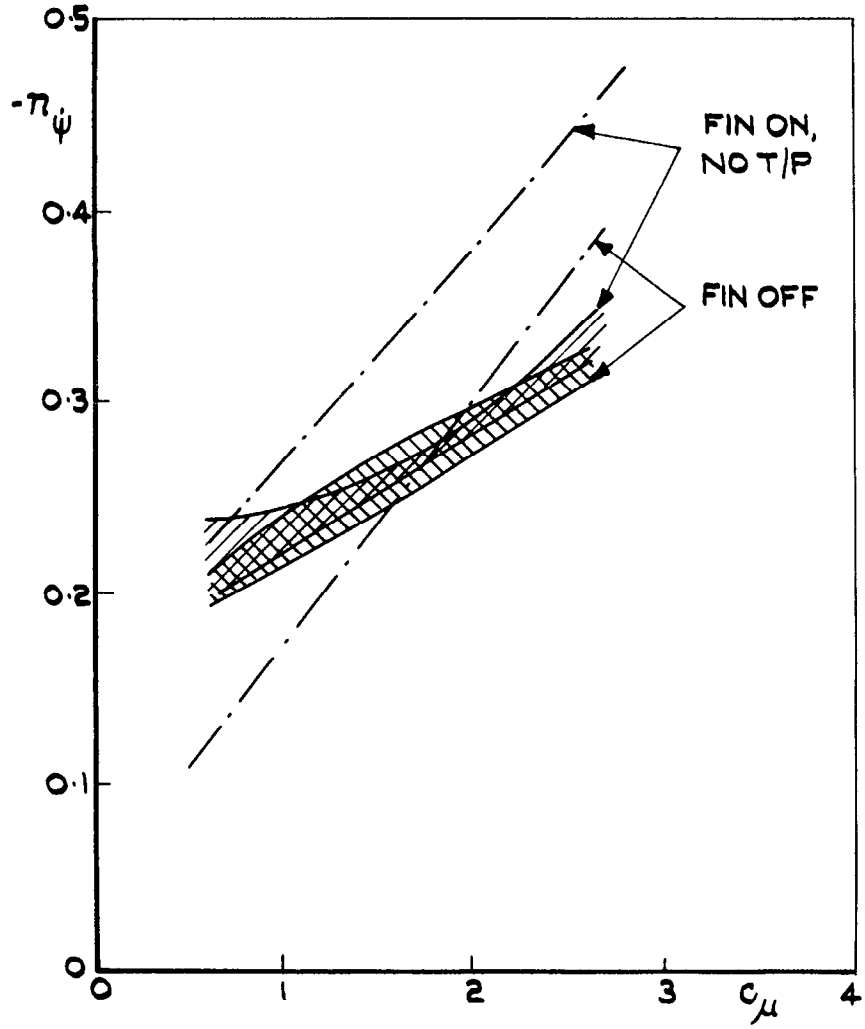

(b) CONTROL ANGLE = 30° ($\theta \triangleq 50°$)

FIG. 19. COMPARISON WITH ESTIMATES AT $\alpha_W = 20°$ $T_{NOM} = 2$ sec.

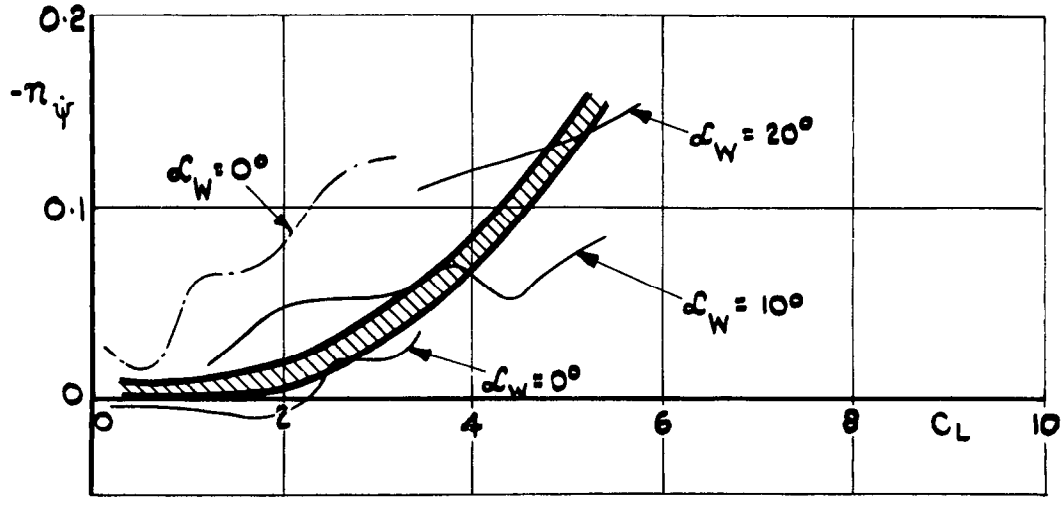

(a) CONTROL ANGLE = 0°($\theta \triangleq 20°$)

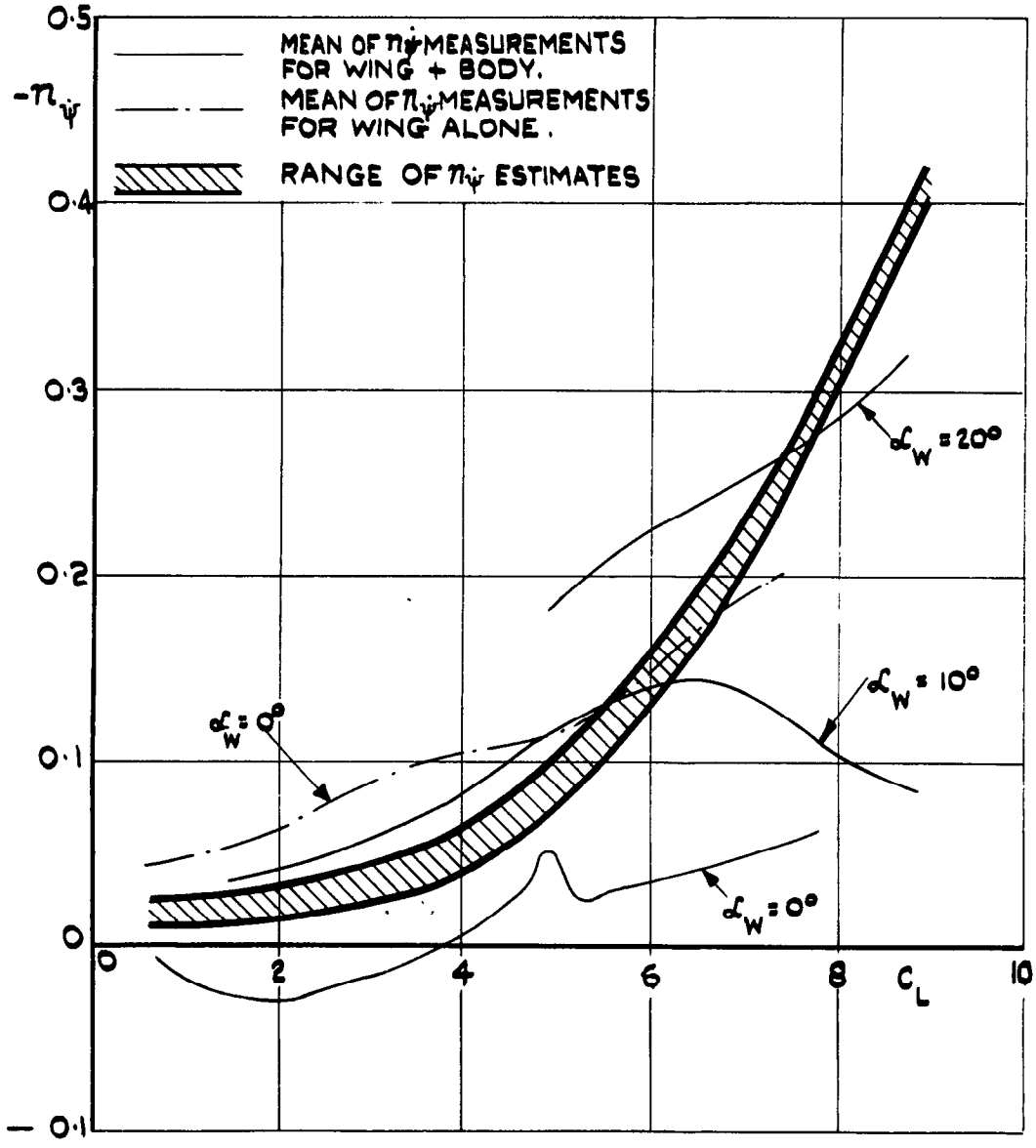

(b) CONTROL ANGLE = 30°($\theta \triangleq 50°$)

FIG. 20. EFFECT OF C_L ON $n_{\dot{\psi}}$, NO FIN. $T_{NOM.}$ = 2 sec.

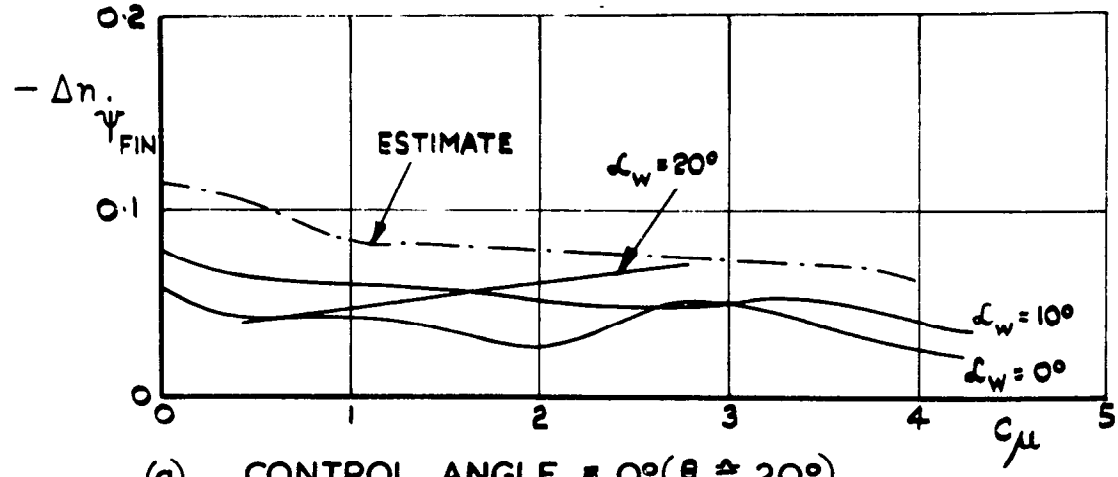

(a) CONTROL ANGLE = 0°($\theta \triangleq 20°$)

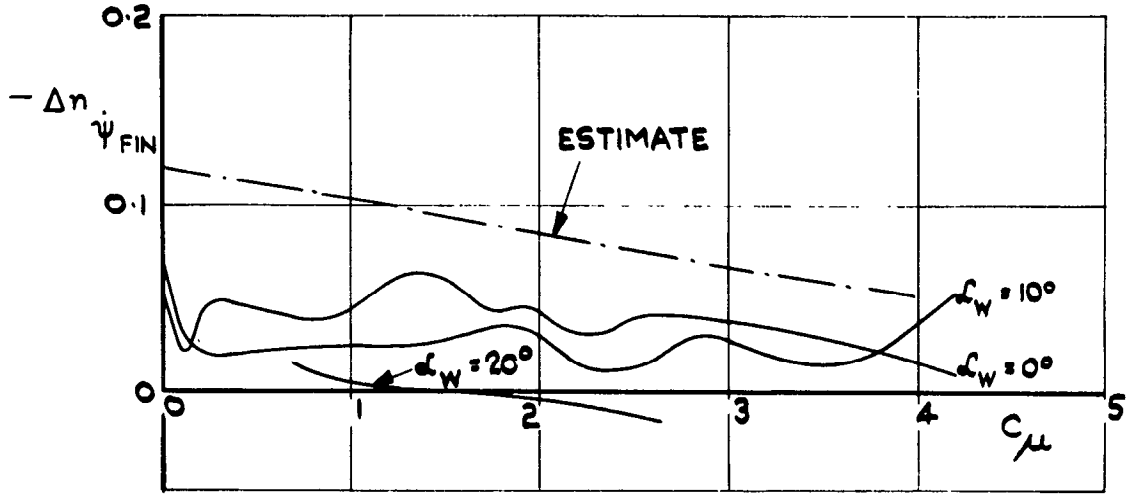

(b) CONTROL ANGLE = 30°($\theta \triangleq 50°$)

FIG. 21. EFFECT OF C_μ ON $\Delta n_{\dot{\psi}}$ DUE TO FIN. (NO TAILPLANE) T_{NOM} = 2sec.

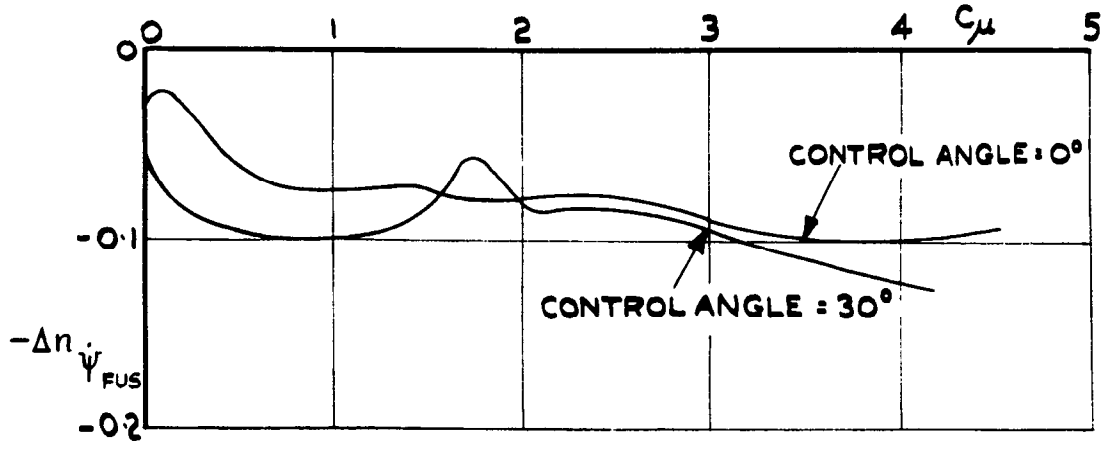

FIG. 22. EFFECT OF C_μ ON $\Delta n_{\dot{\psi}}$ DUE TO FUSELAGE.

Printed in England for Her Majesty's Stationery Office by the Royal Aircraft Establishment, Farnborough. Dd.125875. K4.

A.R.C. C.P. No. 869

Cox, A.P.
Butler, S.F.J.

533.652.6 :
533.6.013.423 :
533.6.013.154 :
533.694.6

LOW-SPEED WIND-TUNNEL MEASUREMENTS OF DAMPING IN YAW ($n_{\dot{\psi}}$) ON AN ASPECT RATIO 9 JET-FLAP COMPLETE MODEL

February 1965

Measurements have been made of the yaw-damping derivative, $n_{\dot{\psi}}$, on an A.R.9 jet-flap complete model, using the free-oscillation technique. The experimental apparatus and procedure is fully described, with the exception of the special air-bearing support system, which has been the subject of a previous Report. Results are given of damping measurements at wing incidences of 0°, 10° and 20° with jet-flap control angles of 0° and 30° and a C_μ range of 0 to 4.2. The effects of the wing, fin, tailplane and fuselage were measured, and it was found that the latter gave a large and

(Over)

A.R.C. C.P. No. 869

Cox, A.P.
Butler, S.F.J.

533.652.6 :
533.6.013.423 :
533.6.013.154 :
533.694.6

LOW-SPEED WIND-TUNNEL MEASUREMENTS OF DAMPING IN YAW ($n_{\dot{\psi}}$) ON AN ASPECT RATIO 9 JET-FLAP COMPLETE MODEL

February 1965

Measurements have been made of the yaw-damping derivative, $n_{\dot{\psi}}$, on an A.R.9 jet-flap complete model, using the free-oscillation technique. The experimental apparatus and procedure is fully described, with the exception of the special air-bearing support system, which has been the subject of a previous Report. Results are given of damping measurements at wing incidences of 0° , 10° and 20° with jet-flap control angles of 0° and 30° and a C_μ range of 0 to 4.2. The effects of the wing, fin, tailplane and fuselage were measured, and it was found that the latter gave a large and

(Over)

A.R.C. C.P. No. 869

Cox, A.P.
Butler, S.F.J.

533.652.6 :
533.6.013.423 :
533.6.013.154 :
533.694.6

LOW-SPEED WIND-TUNNEL MEASUREMENTS OF DAMPING IN YAW ($n_{\dot{\psi}}$) ON AN ASPECT RATIO 9 JET-FLAP COMPLETE MODEL

February 1965

Measurements have been made of the yaw-damping derivative, $n_{\dot{\psi}}$, on an A.R.9 jet-flap complete model, using the free-oscillation technique. The experimental apparatus and procedure is fully described, with the exception of the special air-bearing support system, which has been the subject of a previous Report. Results are given of damping measurements at wing incidences of 0° , 10° and 20° with jet-flap control angles of 0° and 30° and a C_μ range of 0 to 4.2. The effects of the wing, fin, tailplane and fuselage were measured, and it was found that the latter gave a large and

(Over)

DETACHABLE ABSTRACT CARDS

unpredicted destabilising contribution, while damping due to the fin was smaller than the estimated value. Visual observations of the flow in the jet wake showed some correlation with the measured effects.

Comparison of the measured damping for the complete wing + fuselage model with that estimated for the wing-alone, assuming a full-span jet sheet, gave a deceptive measure of agreement, due mainly to the unexpectedly large fuselage contribution.

unpredicted destabilising contribution, while damping due to the fin was smaller than the estimated value. Visual observations of the flow in the jet wake showed some correlation with the measured effects.

Comparison of the measured damping for the complete wing + fuselage model with that estimated for the wing-alone, assuming a full-span jet sheet, gave a deceptive measure of agreement, due mainly to the unexpectedly large fuselage contribution.

unpredicted destabilising contribution, while damping due to the fin was smaller than the estimated value. Visual observations of the flow in the jet wake showed some correlation with the measured effects.

Comparison of the measured damping for the complete wing + fuselage model with that estimated for the wing-alone, assuming a full-span jet sheet, gave a deceptive measure of agreement, due mainly to the unexpectedly large fuselage contribution.

Published by
HER MAJESTY'S STATIONERY OFFICE
To be purchased from
49 High Holborn, London W.C.1
423 Oxford Street, London W.1
13A Castle Street, Edinburgh 2
109 St. Mary Street, Cardiff
Brazennose Street, Manchester 2
50 Fairfax Street, Bristol 1
35 Smallbrook, Ringway, Birmingham 5
80 Chichester Street, Belfast 1
or through any bookseller

S.O. CODE No. 23-9016-69